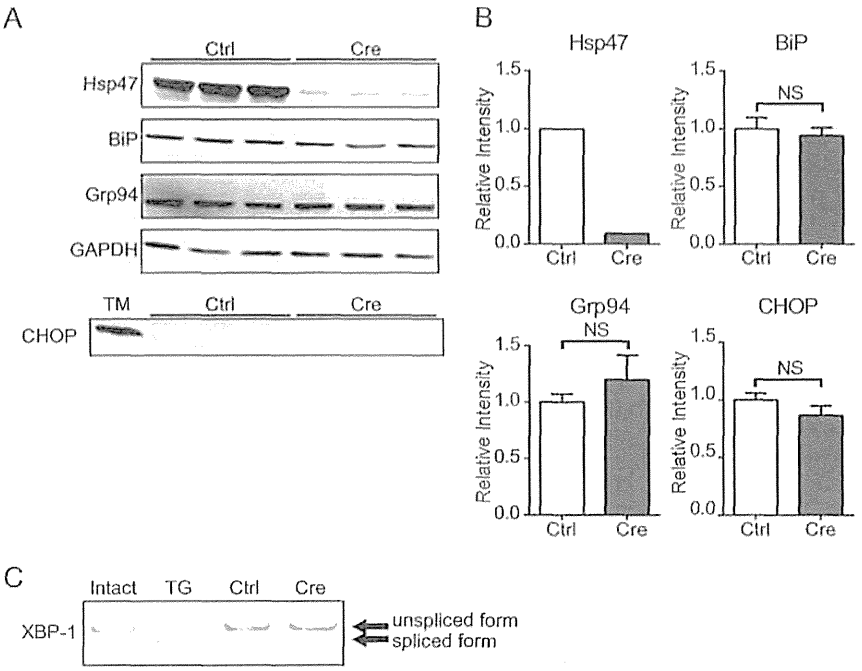

FIGURE 3. **Endoplasmic reticulum stress and apoptosis are not observed in Hsp47-KO HSCs.** *A*, Western blot analyses of activated HSCs infected with AdControl or AdCre at a multiplicity of infection of 25 were performed with the indicated antibodies. HSCs were treated with tunicamycin (*TM*) as a positive control for CHOP detection. *B*, the protein levels of Hsp47, BiP, Grp94, and CHOP in *A* are shown relative to that of GAPDH. Experiments were performed four times independently, and values are means ± S.E. **, $p \leq 0.01$. *NS*, not significant. *C*, RT-PCR for XBP-1 in activated HSCs infected with AdControl or AdCre at a MOI of 25. HSCs were treated with thapsigargin (*TG*) as a positive control for detecting of XBP-1 spliced form. *Ctrl*, control.

the type II collagen promoter (*Col2-cre*). In the current study, HSCs were isolated from *Hsp47*$^{flox/flox}$ mice and activated by culture on a noncoated plastic dish. Hsp47 was depleted in the activated HSCs by infection with an adenovirus encoding Cre recombinase (AdCre). At day 4 after infection, expression of Hsp47 mRNA was decreased in HSCs infected with AdCre to less than 10% of the level in HSCs infected with the control adenovirus (AdControl), so-called control HSCs (Fig. 1, *A* and *B*). This suggests that Hsp47 was almost completely knocked out. At days 4 and 8 after infection, the protein level of Hsp47 in Hsp47-KO HSCs was decreased to ~40% and less than 20% of the level in control HSCs, respectively (Fig. 1, *C* and *D*). At day 12 after infection, the mRNA and protein levels of Hsp47 in Hsp47-KO HSCs were less than 10 and 20% of those in control HSCs, respectively. These results indicate that the *Hsp47* gene was disrupted in activated HSCs by infection with AdCre.

Accumulation of Type I Procollagen in the ER of Hsp47-KO HSCs—The effect of Hsp47 on the maturation of type I collagen in activated HSCs was examined using Hsp47-KO HSCs. The accumulation of extracellular type I collagen was analyzed by immunostaining with an anti-collagen antibody without permeabilizing cells. The level of extracellular collagen was dramatically decreased in Hsp47-KO HSCs, in comparison with control HSCs (Fig. 2*A*). The amount of type I procollagen that accumulated inside cells, as determined by immunoblot analysis, was clearly higher in Hsp47-KO HSCs than in control HSCs (Fig. 2, *B* and *C*). Accumulation of type I procollagen in the detergent-insoluble fraction was hardly observed either in control or Hsp47-KO HSCs. It might be noted that procollagen was clearly detected in the detergent-insoluble fraction in Hsp47-KO MEFs (22). The localization of procollagen within cells was next examined by immunostaining HSCs after they had been permeabilized using Triton X-100. Type I procollagen localized primarily in the Golgi apparatus in control HSCs, as shown by its colocalization with GM130 (*cis*-Golgi marker) (41) but not with protein-disulfide isomerase (ER marker) (42). However, in Hsp47-KO HSCs, the level of type I procollagen in the ER was markedly increased, and this procollagen was also clearly observed in the Golgi apparatus (Fig. 2*D*). These results suggest that in the absence of Hsp47, type I procollagen failed to form the mature form and therefore could not be deposited in the extracellular matrix. Consequently, a portion of procollagen remained in the ER as a detergent-insoluble form in Hsp47-KO HSCs.

Induction of ER Stress and Apoptosis in AdCre-infected HSCs—The accumulation of misfolded proteins and/or detergent-insoluble protein aggregates in the ER reportedly causes ER stress and consequently apoptosis via the induction of CHOP expression, which is up-regulated by PERK in the unfolded protein response pathways (32, 37). The amount of type I procollagen in the ER was greatly increased in Hsp47-KO HSCs (Fig. 2, *B* and *C*); therefore, the induction of ER stress and/or apoptosis was examined in these cells. First, the induction of several stress proteins in the ER, including BiP and GRP94, was examined to determine whether ER stress was induced in AdCre-infected HSCs. Although Hsp47 expression was dramatically decreased in Hsp47-KO HSCs, expression of BiP or Grp94 was not clearly changed (Fig. 3, *A* and *B*). The splicing of XBP-1 by activated IRE1 is known to be induced during ER stress (32). XBP-1 splicing analyzed by RT-PCR was

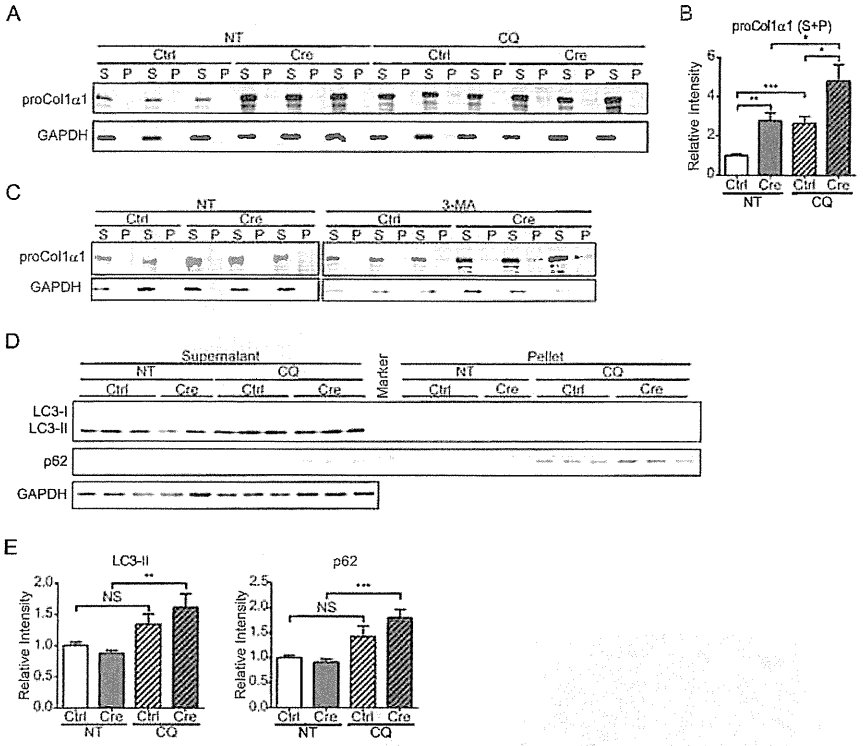

FIGURE 4. **Accumulation of type I procollagen in Hsp47-KO HSCs when autophagy is inhibited.** *A*, the protein levels of type I procollagen α1 and GAPDH in activated HSCs infected with AdControl or AdCre at a MOI of 25 and treated with or without CQ were detected by immunoblotting with anti-type I collagen (proCol1α1) and anti-GAPDH antibodies. Cell lysates were separated by centrifugation to generate detergent-soluble (*S*) and detergent-insoluble (*P*) fractions. *B*, the protein level of type I procollagen α1 in *A* is shown relative to that of GAPDH. Experiments were performed eight times independently. *C*, the protein levels of type I procollagen α1 and GAPDH in activated HSCs infected with AdControl or AdCre at a MOI of 25 and treated with or without 3-MA were detected by immunoblotting with anti-type I collagen (proCol1a1) and anti-GAPDH antibodies. Cell lysates were separated by centrifugation to generate detergent-soluble (*S*) and detergent-insoluble (*P*) fractions. The samples representing the detergent-insoluble fraction are 5-fold concentrated in comparison with the detergent-soluble fraction. *D*, Western blot analyses of LC3, p62, and GAPDH in activated HSCs infected with AdControl or AdCre at a MOI of 25 and treated with or without CQ were performed with the indicated antibodies. Cell lysates were separated by centrifugation to generate detergent-soluble (supernatant) and detergent-insoluble (pellet) fractions. *E*, the protein levels of LC3-II and p62 in supernatant fraction in *D* are shown relative to that of GAPDH. Experiments were performed nine times independently. All values are means ± S.E. *, $p \leq 0.05$; **, $p \leq 0.01$; ***, $p \leq 0.001$. *NS*, not significant; *NT*, not treated; *Ctrl*, control.

not observed in Hsp47-KO HSCs (Fig. 3*C*). The induction of CHOP (Fig. 3, *A* and *B*) and caspase-3 (data not shown) expression, which are apoptosis makers, was also not detected in Hsp47-KO HSCs. These results suggest that neither ER stress nor apoptosis were induced in Hsp47-KO HSCs. We previously reported that ER stress induces apoptosis in MEFs in which Hsp47 is disrupted by homologous recombination (22). However, aggregates of misfolded procollagen in the ER of these cells are degraded by autophagy (22). Therefore, the induction of apoptosis in these cells was considered to be accentuate under the inhibition of autophagy. Thus, the effect of autophagy inhibition on the induction of ER stress and apoptosis in Hsp47-KO HSCs was next examined by treating these cells with inhibitors of autophagy.

HSCs were treated with CQ, which inhibits autophagy by preventing acidification of lysosomes (43). First, the accumulation of type I procollagen was examined by immunoblot analysis of CQ-treated cells. Type I procollagen accumulated in CQ-treated control HSCs (Fig. 4, *A* and *B*). The level of procollagen was significantly higher in Hsp47-KO HSCs than in control HSCs in the absence of CQ treatment, and the level of procollagen in Hsp47-KO HSCs was greatly increased following CQ treatment. Furthermore, the amount of procollagen was modestly higher in the detergent-insoluble fraction of CQ-treated Hsp47-KO HSCs than in that of untreated Hsp47-KO HSCs (Fig. 4*A*). The increase of procollagen in Hsp47-KO HSCs was also observed when autophagy was inhibited with 3-MA, another autophagy inhibitor that inhibits type III phosphatidylinositol 3-kinases (44) (Fig. 4*C*). After treatment with CQ for 24 h on day 12 after infection with AdControl or AdCre, the levels of LC3 and p62, which are autophagy markers, were determined by immunoblot analysis. During activation of autophagy, LC3, a membrane component of the autophagosome, is converted from LC3-I to LC3-II by the conjugation of phosphatidylethanolamine (45). In control HSCs, CQ treatment did not significantly affect the levels of p62 and LC3-II (Fig. 4, *D* and *E*). By contrast, in Hsp47-KO HSCs, the levels of LC3-II and p62 were significantly increased by CQ treatment. These results clearly indicated that autophagy was up-regulated in Hsp47-KO HSCs (Fig. 4, *D* and *E*), which is consistent with our previous work (22). The levels of BiP and Grp94 were significantly increased in Hsp47-KO HSCs when autophagy was inhibited, whereas this was not observed in control HSCs (Fig. 5, *A*–*C*). CHOP was also up-regulated in Hsp47-KO HSCs, but not in control HSCs, when autophagy was inhibited (Fig. 5, *A* and *B*). The activity of caspase-3 was examined using a fluores-

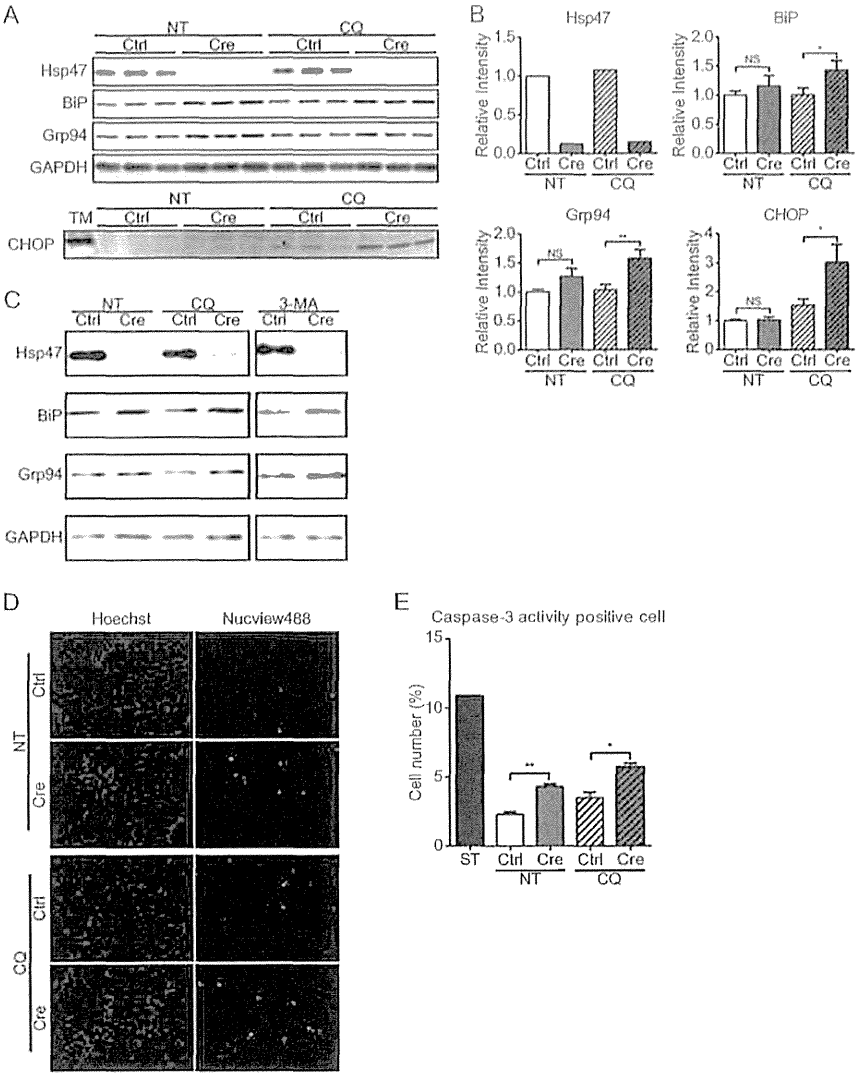

FIGURE 5. **Induction of endoplasmic reticulum stress and apoptosis in Hsp47-KO HSCs when autophagy is inhibited.** *A*, the protein levels of Hsp47, BiP, Grp94, CHOP, and GAPDH in activated HSCs infected with AdControl or AdCre at a MOI of 25 and treated with or without CQ were detected by Western blot analyses using the indicated antibodies. HSCs were treated with tunicamycin (*TM*) as positive control for CHOP detection. *B*, the protein levels of Hsp47, BiP, Grp94, and CHOP in *A* are shown relative to that of GAPDH. Experiments were performed nine times independently. *C*, the protein levels of Hsp47, BiP, Grp94, and GAPDH in activated HSCs infected with AdControl or AdCre at a MOI of 25 and treated with or without CQ and 3-MA were detected by Western blot analyses using the indicated antibodies. *D*, activation of caspase-3 in activated HSCs infected with AdCre or AdControl at a MOI of 25 and treated with or without CQ was analyzed using the Nucview488 caspase-3/7 substrate (*green*) and Hoechst 33342 (*blue*). *E*, the ratio of caspase-3 activity-positive cells to Hoechst 33342-positive cells in *D* is shown. HSCs were treated with staurosporine (*ST*) as positive control for apoptosis. Experiments were performed three times independently. All values are means ± S.E. *, $p \leq 0.05$; **, $p \leq 0.01$. *NS*, not significant; *NT*, not treated; *Ctrl*, control.

cent marker-conjugated caspase-3 substrate (Fig. 5, *D* and *E*). The number of Hsp47-KO HSCs with caspase-3 activity was increased even in the absence of CQ (Fig. 5*E*), whereas the CHOP induction was not changed (Fig. 5*B*). CQ treatment increased the numbers of control and Hsp47-KO HSCs that exhibited caspase-3 activity (Fig. 5*E*). These results suggest that ER stress was induced in Hsp47-KO HSCs through the accumulation of type I procollagen in the ER when autophagy was inhibited and caused the apoptosis in activated HSCs.

DISCUSSION

Since we first identified Hsp47 as a collagen-specific molecular chaperone residing in the ER of mammalian cells (13, 15), correlational expression analysis of Hsp47 and various types of collagens has been reported in numerous tissues (15) and collagen-related diseases including fibrosis (24, 25). This correlational expression of Hsp47 and collagens is important for the potential treatment of fibrotic disorders because down-regulation of Hsp47 expression by RNAi or antisense RNA methods markedly delays the progression of fibrosis and concomitantly reduces the level of collagen in the extracellular matrix (27–31). Recently, knockdown of Hsp47 in the HSCs of rat, which was achieved using a drug delivery system to target RNAi specifically to these cells, was shown to markedly prevent the progression of experimental liver fibrosis (28, 30). In this report, apoptotic death of HSCs in rats treated with Hsp47-targeting RNAi

was suggested to be a major reason underlying the dramatic therapeutic effects on liver fibrosis.

We previously reported that disruption of the *Hsp47* gene in mice causes improper molecular maturation of type I and/or IV procollagens and the accumulation of these molecules in the ER as detergent-insoluble aggregates that are not secreted (17–19). In Hsp47-KO mouse embryos, ER stress-mediated apoptotic cell death is observed in various tissues and MEFs (18, 20, 22). Thus, we hypothesized that the abnormal accumulation of misfolded and/or aggregated procollagens in the ER of mice treated with Hsp47-targeting RNAi might cause ER stress, leading to the expression of CHOP and other apoptosis-inducing genes, and that this ER stress might be the major reason underlying the apoptosis of HSCs.

To address this issue, we established an inducible knock-out system for the *Hsp47* gene by infecting activated HSCs from *Hsp47*$^{flox/flox}$ mouse liver with AdCre. ER stress was not observed in activated control or Hsp47-KO HSCs (Figs. 3 and 5), which is inconsistent with our previous results in Hsp47-KO MEFs (22). This apparent discrepancy may be due to the difference in the basal expression level of procollagen; it is higher in MEFs compared with that in HSCs. In addition, the autophagy was reported to be activated in HSCs (48, 49), which attenuates the induction of ER stress in HSCs, because the misfolded proteins in the ER could be eliminated by autophagy (ER-phagy). We previously reported that misfolded procollagen trimers in the ER are degraded by autophagy, whereas misfolded single procollagen α-chains are degraded by ER-associated degradation (22, 46, 47). Thus, we treated activated HSCs with inhibitors of autophagy. Upon treatment with autophagy inhibitor, the level of procollagens in the ER was increased in both control and Hsp47-KO HSCs (Fig. 4, *A–C*). It suggests that a part of procollagens was degraded through autophagic pathway. As mentioned above, it was reported recently that the up-regulation of autophagy is required for the activation of hepatic stellate cell (48, 49). It is conceivable that this higher activity of autophagy may be responsible for degrading procollagen even in control HSCs. The increase in the accumulation of procollagens in the ER of CQ-treated cells was reflected by the induction of ER stress, which was detected by the increased levels of BiP and Grp94 (Fig. 5, *A–C*). It should be noted that the increased accumulation of procollagens caused ER stress in Hsp47-KO HSCs, but not in control HSCs (Fig. 5, *A–C*), which suggests that the molecular conformation of accumulated procollagens differs according to whether Hsp47 is present or absent. This is supported by our observation that autophagy was up-regulated much more in Hsp47-KO HSCs than in control HSCs (Fig. 4, *D* and *E*). ER stress in Hsp47-KO HSCs induced apoptosis, which was detected by increases in the level of CHOP and the activity of caspase-3 (Fig. 5).

Thus, we clearly showed that procollagens that accumulate in the ER of activated HSCs because of the absence of Hsp47 can be degraded by autophagy. However, when autophagy is blocked or overwhelmed by the excess accumulation of misfolded procollagens, activated HSCs undergo apoptosis.

During regression of fibrosis, half of the activated HSCs undergo apoptosis, and the other half revert back to inactivated HSCs (50). Reinactivated HSCs are more sensitive to inflammatory cytokines and are more easily activated than quiescent HSCs. Therefore, reinactivated HSCs are regarded as a risk factor for fibrosis. Thus, immediate and sufficient elimination of activated HSCs is important for the treatment of fibrosis. We showed that apoptosis was induced in activated HSCs by a combination of Hsp47 KO and inhibition of autophagy.

The observations of this study are important with regards to the use of Hsp47 down-regulation as a therapeutic strategy for various fibroses, including liver cirrhosis. Down-regulation of Hsp47 blocks the deposition of procollagens in the extracellular matrix by activated HSCs, which decreases the level of collagens in fibrotic tissues. In addition, prevention of the secretion of procollagens from the ER causes these proteins to accumulate in the ER, which leads to apoptosis of HSCs, the major collagen-producing cells in the liver. Thus, down-regulation of Hsp47 can alleviate fibrosis in two concomitant ways: by inhibiting the secretion of collagen and by inducing apoptosis in collagen-producing cells. This sheds light on a new strategy to treat fibrosis.

Acknowledgments—We thank Dr. Yoshiya Kawaguchi and Dr. Kenichiro Furuyama for providing professional instructions with isolation of HSCs.

REFERENCES

1. Friedman, S. L. (2008) Mechanisms of hepatic fibrogenesis. *Gastroenterology* **134,** 1655–1669
2. Wake, K. (1980) Perisinusoidal stellate cells (fat-storing cells, interstitial cells, lipocytes), their related structure in and around the liver sinusoids, and vitamin A-storing cells in extrahepatic organs. *Int. Rev. Cytol.* **66,** 303–353
3. Friedman, S. L. (2008) Hepatic stellate cells: protean, multifunctional, and enigmatic cells of the liver. *Physiol. Rev.* **88,** 125–172
4. Chessler, S. D., and Byers, P. H. (1993) BiP binds type I procollagen pro alpha chains with mutations in the carboxyl-terminal propeptide synthesized by cells from patients with osteogenesis imperfecta. *J. Biol. Chem.* **268,** 18226–18233
5. Ferreira, L. R., Norris, K., Smith, T., Hebert, C., and Sauk, J. J. (1994) Association of Hsp47, Grp78, and Grp94 with procollagen supports the successive or coupled action of molecular chaperones. *J. Cell. Biochem.* **56,** 518–526
6. Lamandé, S. R., Chessler, S. D., Golub, S. B., Byers, P. H., Chan, D., Cole, W. G., Sillence, D. O., and Bateman, J. F. (1995) Endoplasmic reticulum-mediated quality control of type I collagen production by cells from osteogenesis imperfecta patients with mutations in the pro alpha 1 (I) chain carboxyl-terminal propeptide which impair subunit assembly. *J. Biol. Chem.* **270,** 8642–8649
7. Wilson, R., Lees, J. F., and Bulleid, N. J. (1998) Protein disulfide isomerase acts as a molecular chaperone during the assembly of procollagen. *J. Biol. Chem.* **273,** 9637–9643
8. Nagata, K. (2003) HSP47 as a collagen-specific molecular chaperone: function and expression in normal mouse development. *Semin. Cell Dev. Biol.* **14,** 275–282
9. Walmsley, A. R., Batten, M. R., Lad, U., and Bulleid, N. J. (1999) Intracellular retention of procollagen within the endoplasmic reticulum is mediated by prolyl 4-hydroxylase. *J. Biol. Chem.* **274,** 14884–14892
10. Smith, T., Ferreira, L. R., Hebert, C., Norris, K., and Sauk, J. J. (1995) Hsp47 and cyclophilin B traverse the endoplasmic reticulum with procollagen into pre-Golgi intermediate vesicles: a role for Hsp47 and cyclophilin B in the export of procollagen from the endoplasmic reticulum. *J. Biol. Chem.* **270,** 18323–18328
11. Vranka, J. A., Sakai, L. Y., and Bächinger, H. P. (2004) Prolyl 3-hydroxylase 1, enzyme characterization and identification of a novel family of enzymes. *J. Biol. Chem.* **279,** 23615–23621
12. Ishikawa, Y., Wirz, J., Vranka, J. A., Nagata, K., and Bächinger, H. P. (2009) Biochemical characterization of the prolyl 3-hydroxylase 1.cartilage-associated protein·cyclophilin B complex. *J. Biol. Chem.* **284,** 17641–17647

13. Nagata, K., Saga, S., and Yamada, K. M. (1986) A major collagen-binding protein of chick embryo fibroblasts is a novel heat shock protein. *J. Cell Biol.* **103,** 223–229
14. Saga, S., Nagata, K., Chen, W. T., and Yamada, K. M. (1987) pH-dependent function, purification, and intracellular location of a major collagen-binding glycoprotein. *J. Cell Biol.* **105,** 517–527
15. Nagata, K. (1996) Hsp47: a collagen-specific molecular chaperone. *Trends Biochem. Sci.* **21,** 22–26
16. Tasab, M., Batten, M. R., and Bulleid, N. J. (2000) Hsp47: a molecular chaperone that interacts with and stabilizes correctly-folded procollagen. *EMBO J.* **19,** 2204–2211
17. Nagai, N., Hosokawa, M., Itohara, S., Adachi, E., Matsushita, T., Hosokawa, N., and Nagata, K. (2000) Embryonic lethality of molecular chaperone hsp47 knockout mice is associated with defects in collagen biosynthesis. *J. Cell Biol.* **150,** 1499–1506
18. Marutani, T., Yamamoto, A., Nagai, N., Kubota, H., and Nagata, K. (2004) Accumulation of type IV collagen in dilated ER leads to apoptosis in Hsp47-knockout mouse embryos via induction of CHOP. *J. Cell Sci.* **117,** 5913–5922
19. Matsuoka, Y., Kubota, H., Adachi, E., Nagai, N., Marutani, T., Hosokawa, N., and Nagata, K. (2004) Insufficient folding of type IV collagen and formation of abnormal basement membrane-like structure in embryoid bodies derived from Hsp47-null embryonic stem cells. *Mol. Biol. Cell* **15,** 4467–4475
20. Masago, Y., Hosoya, A., Kawasaki, K., Kawano, S., Nasu, A., Toguchida, J., Fujita, K., Nakamura, H., Kondoh, G., and Nagata, K. (2012) The molecular chaperone Hsp47 is essential for cartilage and endochondral bone formation. *J. Cell Sci.* **125,** 1118–1128
21. Ishida, Y., Kubota, H., Yamamoto, A., Kitamura, A., Bächinger, H. P., and Nagata, K. (2006) Type I collagen in Hsp47-null cells is aggregated in endoplasmic reticulum and deficient in *N*-propeptide processing and fibrillogenesis. *Mol. Biol. Cell* **17,** 2346–2355
22. Ishida, Y., Yamamoto, A., Kitamura, A., Lamandé, S. R., Yoshimori, T., Bateman, J. F., Kubota, H., and Nagata, K. (2009) Autophagic elimination of misfolded procollagen aggregates in the endoplasmic reticulum as a means of cell protection. *Mol. Biol. Cell* **20,** 2744–2754
23. Tanida, I. (2011) Autophagosome formation and molecular mechanism of autophagy. *Antioxid. Redox. Signal.* **14,** 2201–2214
24. Masuda, H., Fukumoto, M., Hirayoshi, K., and Nagata, K. (1994) Coexpression of the collagen-binding stress protein HSP47 gene and the alpha 1(I) and alpha 1(III) collagen genes in carbon tetrachloride-induced rat liver fibrosis. *J. Clin. Invest.* **94,** 2481–2488
25. Naitoh, M., Hosokawa, N., Kubota, H., Tanaka, T., Shirane, H., Sawada, M., Nishimura, Y., and Nagata, K. (2001) Upregulation of HSP47 and collagen type III in the dermal fibrotic disease, keloid. *Biochem. Biophys. Res. Commun.* **280,** 1316–1322
26. Nakai, A., Satoh, M., Hirayoshi, K., and Nagata, K. (1992) Involvement of the stress protein HSP47 in procollagen processing in the endoplasmic reticulum. *J. Cell Biol.* **117,** 903–914
27. Sunamoto, M., Kuze, K., Tsuji, H., Ohishi, N., Yagi, K., Nagata, K., Kita, T., and Doi, T. (1998) Antisense oligonucleotides against collagen-binding stress protein HSP47 suppress collagen accumulation in experimental glomerulonephritis. *Lab. Invest.* **78,** 967–972
28. Sato, Y., Murase, K., Kato, J., Kobune, M., Sato, T., Kawano, Y., Takimoto, R., Takada, K., Miyanishi, K., Matsunaga, T., Takayama, T., and Niitsu, Y. (2008) Resolution of liver cirrhosis using vitamin A-coupled liposomes to deliver siRNA against a collagen-specific chaperone. *Nat. Biotechnol.* **26,** 431–442
29. Kitamura, H., Yamamoto, S., Nakase, H., Matsuura, M., Honzawa, Y., Matsumura, K., Takeda, Y., Uza, N., Nagata, K., and Chiba, T. (2011) Role of heat shock protein 47 in intestinal fibrosis of experimental colitis. *Biochem. Biophys. Res. Commun.* **404,** 599–604
30. Ishiwatari, H., Sato, Y., Murase, K., Yoneda, A., Fujita, R., Nishita, H., Birukawa, N. K., Hayashi, T., Sato, T., Miyanishi, K., Takimoto, R., Kobune, M., Ota, S., Kimura, Y., Hirata, K., Kato, J., and Niitsu, Y. (2013) Treatment of pancreatic fibrosis with siRNA against a collagen-specific chaperone in vitamin A-coupled liposomes. *Gut* **62,** 1328–1339
31. Honzawa, Y., Nakase, H., Shiokawa, M., Yoshino, T., Imaeda, H., Matsuura, M., Kodama, Y., Ikeuchi, H., Andoh, A., Sakai, Y., Nagata, K., and Chiba, T. (2014) Involvement of interleukin-17A-induced expression of heat shock protein 47 in intestinal fibrosis in Crohn's disease. *Gut* **63,** 1902–1912
32. Walter, P., and Ron, D. (2011) The unfolded protein response: from stress pathway to homeostatic regulation. *Science* **334,** 1081–1086
33. Harding, H. P., Zhang, Y., and Ron, D. (1999) Protein translation and folding are coupled by an endoplasmic-reticulum-resident kinase. *Nature* **397,** 271–274
34. Haze, K., Yoshida, H., Yanagi, H., Yura, T., and Mori, K. (1999) Mammalian transcription factor ATF6 is synthesized as a transmembrane protein and activated by proteolysis in response to endoplasmic reticulum stress. *Mol. Biol. Cell* **10,** 3787–3799
35. Cox, J. S., Shamu, C. E., and Walter, P. (1993) Transcriptional induction of genes encoding endoplasmic reticulum resident proteins requires a transmembrane protein kinase. *Cell* **73,** 1197–1206
36. Mori, K., Ma, W., Gething, M. J., and Sambrook, J. (1993) A transmembrane protein with a cdc2+/CDC28-related kinase activity is required for signaling from the ER to the nucleus. *Cell* **74,** 743–756
37. Gotoh, T., and Mori, M. (2006) Nitric oxide and endoplasmic reticulum stress. *Arterioscler. Thromb. Vasc. Biol.* **26,** 1439–1446
38. Radaeva, S., Wang, L., Radaev, S., Jeong, W. I., Park, O., and Gao, B. (2007) Retinoic acid signaling sensitizes hepatic stellate cells to NK cell killing via upregulation of NK cell activating ligand RAE1. *Am. J. Physiol. Gastrointest. Liver Physiol.* **293,** G809–G816
39. Kinoshita, K., Iimuro, Y., Fujimoto, J., Inagaki, Y., Namikawa, K., Kiyama, H., Nakajima, Y., Otogawa, K., Kawada, N., Friedman, S. L., and Ikeda, K. (2007) Targeted and regulable expression of transgenes in hepatic stellate cells and myofibroblasts in culture and *in vivo* using an adenoviral Cre/loxP system to antagonise hepatic fibrosis. *Gut* **56,** 396–404
40. Laemmli, U. K. (1970) Cleavage of structural proteins during the assembly of the head of bacteriophage T4. *Nature* **227,** 680–685
41. Perez, F., Pernet-Gallay, K., Nizak, C., Goodson, H. V., Kreis, T. E., and Goud, B. (2002) CLIPR-59, a new *trans*-Golgi/TGN cytoplasmic linker protein belonging to the CLIP-170 family. *J. Cell Biol.* **156,** 631–642
42. Mehtani, S., Gong, Q., Panella, J., Subbiah, S., Peffley, D. M., and Frankfater, A. (1998) In vivo expression of an alternatively spliced human tumor message that encodes a truncated form of cathepsin B. Subcellular distribution of the truncated enzyme in COS cells. *J. Biol. Chem.* **273,** 13236–13244
43. Steinman, R. M., Mellman, I. S., Muller, W. A., and Cohn, Z. A. (1983) Endocytosis and the recycling of plasma membrane. *J. Cell Biol.* **96,** 1–27
44. Seglen, P. O., and Gordon, P. B. (1982) 3-Methyladenine: specific inhibitor of autophagic/lysosomal protein degradation in isolated rat hepatocytes. *Proc. Natl. Acad. Sci. U.S.A.* **79,** 1889–1892
45. Kabeya, Y., Mizushima, N., Ueno, T., Yamamoto, A., Kirisako, T., Noda, T., Kominami, E., Ohsumi, Y., and Yoshimori, T. (2000) LC3, a mammalian homologue of yeast Apg8p, is localized in autophagosome membranes after processing. *EMBO J.* **19,** 5720–5728
46. Fitzgerald, J., Lamandé, S. R., and Bateman, J. F. (1999) Proteasomal degradation of unassembled mutant type I collagen pro-alpha1(I) chains. *J. Biol. Chem.* **274,** 27392–27398
47. Lamandé, S. R., and Bateman, J. F. (1993) A type I collagen reporter gene construct for protein engineering studies. Functional equivalence of transfected reporter COL1A1 and endogenous gene products during biosynthesis and in vitro extracellular matrix accumulation. *Biochem. J.* **293,** 387–394
48. Thoen, L. F., Guimarães, E. L., Dollé, L., Mannaerts, I., Najimi, M., Sokal, E., and van Grunsven, L. A. (2011) A role for autophagy during hepatic stellate cell activation. *J. Hepatol.* **55,** 1353–1360
49. Hernández-Gea, V., Ghiassi-Nejad, Z., Rozenfeld, R., Gordon, R., Fiel, M. I., Yue, Z., Czaja, M. J., and Friedman, S. L. (2012) Autophagy releases lipid that promotes fibrogenesis by activated hepatic stellate cells in mice and in human tissues. *Gastroenterology* **142,** 938–946
50. Kisseleva, T., Cong, M., Paik, Y., Scholten, D., Jiang, C., Benner, C., Iwaisako, K., Moore-Morris, T., Scott, B., Tsukamoto, H., Evans, S. M., Dillmann, W., Glass, C. K., and Brenner, D. A. (2012) Myofibroblasts revert to an inactive phenotype during regression of liver fibrosis. *Proc. Natl. Acad. Sci. U.S.A.* **109,** 9448–9453

Protein Structure and Folding:

Deletion of the Collagen-specific Molecular Chaperone Hsp47 Causes Endoplasmic Reticulum Stress-mediated Apoptosis of Hepatic Stellate Cells

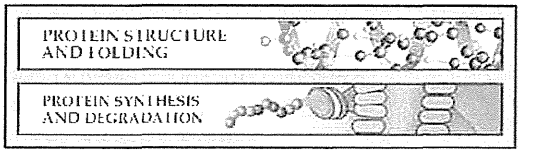

Kunito Kawasaki, Ryo Ushioda, Shinya Ito, Kazuo Ikeda, Yusaku Masago and Kazuhiro Nagata

J. Biol. Chem. 2015, 290:3639-3646.
doi: 10.1074/jbc.M114.592139 originally published online December 18, 2014

JOURNAL OF INTERFERON & CYTOKINE RESEARCH
Volume 35, Number 5, 2015

DOI: 10.1089/jir.2014.0113

Murine Herc6 Plays a Critical Role in Protein ISGylation *In Vivo* and Has an ISGylation-Independent Function in Seminal Vesicles

Kei-ichiro Arimoto,[1] Takayuki Hishiki,[2] Hiroshi Kiyonari,[3] Takaya Abe,[3] Chuyi Cheng,[4] Ming Yan,[1] Jun-Bao Fan,[1] Mitsuru Futakuchi,[5] Hiroyuki Tsuda,[6] Yoshiki Murakami,[7] Hideyuki Suzuki,[8] Dong-Er Zhang,[1,9] and Kunitada Shimotohno[10]

ISG15 conjugation (ISGylation) to proteins is a multistep process involving interferon (IFN)-inducible UBE1L (E1), UbcH8 (E2), and ISG15 E3 ligases (E3s). Studies performed over the past several years have shown that ISGylation plays a pivotal role in the host antiviral response against certain viruses. Recent *in vitro* studies revealed that human Herc5 and mouse Herc6 are major ISG15 E3 ligases, respectively. However, the global function of Herc5/6 proteins *in vivo* still remains unclear. Here, we report generation and initial characterization of Herc6 knockout mice. Substantial reductions of ISGylation were observed in Herc6-deficient cells after polyinosinic-polycytidylic acid double-stranded RNA injection of mice or IFN treatment of cells. On the other hand, Herc6-deficient cells and wild-type (WT) cells had similar responses to IFN stimulation, Sendai virus (Z strain) infection, and vesicular stomatitis virus infection. These results indicate that Herc6 does not play a critical role in antiviral defense of these viral infections in mice. Interestingly, male Herc6-deficient mice showed seminal vesicle hypertrophy. No such problem was detected in WT and ISG15 activating enzyme Ube1L-deficient mice. These results suggest that in addition to promoting protein ISGylation, Herc6 has a novel and protein ISGylation-independent function in the male reproductive system.

Introduction

ISG15 is a 17 kDa ubiquitin-like modifier. Its expression is rapidly induced by type I interferon (IFN) (Bedford and others 2011). Similar to ubiquitin, ISG15 is conjugated to lysines on broad target proteins through the reaction of specific E1-activating (UBE1L), E2-conjugating (UbcH8), and E3-ligase enzymes (Yuan and Krug 2001; Kim and others 2004; Dastur and others 2006; Wong and others 2006). The deconjugation of ISG15 from cellular proteins is carried out by USP18 (Burkart and others 2013). Previous *in vitro* knockdown studies suggested that human Herc5 and mouse Herc6 are the main ISG15 E3 ligases to mediate global conjugation in human cells and mouse cells, respectively (Wong and others 2006; Oudshoorn and others 2012). Mice do not possess the Herc5 gene among the Herc family genes. Human Herc6, which is the closest relative to human Herc5, was devoid of any ISG15 E3 ligase activity (Hochrainer and others 2005; Dastur and others 2006; Oudshoorn and others 2012).

ISG15-mediated antiviral activity against influenza, herpes, and Sindbis virus has been shown *in vivo* by means of infections in ISG15$^{-/-}$ and UBE1L$^{-/-}$ mice (Lenschow and others 2005, 2007; Lai and others 2009; Lenschow 2010). In addition, *in vitro* studies for either the overexpression of ISG15 or knockdown of ISG15 using siRNA have implicated ISGylation in the regulation of influenza B virus, vaccinia virus, Sindbis virus, herpes simplex-1 virus, Sendai virus, and Japanese

[1]Moores UCSD Cancer Center, University of California, San Diego, La Jolla, California.
[2]Laboratory of Primate Model, Experimental Research Center for Infectious Diseases, Institute for Virus Research, Kyoto University, Sakyo-ku, Kyoto, Japan.
[3]Laboratory for Animal Resources and Genetic Engineering, RIKEN Center for Developmental Biology (CDB), Kobe, Hyogo, Japan.
[4]Division of Biological Sciences, University of California, San Diego, La Jolla, California.
[5]Department of Molecular Toxicology, Graduate School of Medical Sciences, Nagoya City University, Nagoya, Aichi, Japan.
[6]Laboratory of Nanotoxicology Project, Nagoya City University, Nagoya, Aichi, Japan.
[7]Department of Hepatology, Graduate School of Medicine, Osaka City University, Osaka-shi, Osaka, Japan.
[8]Oriental Bio Service, Inc., Kobe BM Laboratory, Kobe-shi, Hyogo, Japan.
[9]Department of Pathology, University of California, San Diego, La Jolla, California.
[10]Research Center for Hepatitis and Immunology, National Center for Global Health and Medicine, Ichikawa-shi, Chiba, Japan.

encephalitis virus, as well as in the release of virus-like particles derived from HIV-1 and avian sarcoma leukosis virus (Okumura and others 2006, 2008; Guerra and others 2008; Malakhova and Zhang 2008; Hsiang and others 2009; Hsiao and others 2010; Lenschow 2010; Pincetic and others 2010). Although the mechanism by which ISG15 is regulating viral growth is still unknown for the majority of these viruses, it has been reported that ISG15 achieves its antiviral role by conjugating to target proteins, including both host proteins and viral proteins, and altering their functions. For example, ISG15 can be conjugated to host antiviral protein interferon regulatory factor 3 (IRF3) and, thus, stabilize IRF3 by inhibiting its interaction with peptidyl-prolyl cis-trans isomerase NIMA-interacting 1 (PIN1), a protein that promotes IRF3 ubiquitination and degradation (Shi and others 2010). In most overexpression studies, ISG15 and its conjugation-related enzymes have been coexpressed, suggesting that ISG15 conjugation to target proteins is required for these antiviral effects. Despite these observations with either *in vivo* or *in vitro* studies, there are some controversial phenotypes: No differences in viral growth of influenza A, herpes simplex virus-1, Sindbis, and wild-type (WT) vaccinia virus in ISG15$^{-/-}$ mouse embryonic fibroblast cells (MEFs) and vesicular stomatitis virus (VSV) in UBE1L$^{-/-}$ MEFs have also been reported (Osiak and others 2005; Kim and others 2006; Lenschow and others 2007; Guerra and others 2008).

A recent report indicated that human Herc5 globally targets *de novo* synthesized proteins for ISG15 conjugation, thereby making viral proteins major targets for ISGylation (Durfee and others 2010). However, the question remains whether Herc5 and global ISGylation are important for antiviral activity *in vivo*, as ISGylation-mediated antiviral effects might be due to other minor ISG15 E3 ligases with more narrow specificity, such as estrogen-responsive finger protein (EFP, also called TRIM25) (Park and others 2014). Since there is no mouse ortholog of human HERC5, the other members of HERC family proteins have been examined for ISG15 E3 activity. A recent report shows that Herc6 knockdown in mouse L929 cells abolished global ISGylation, whereas its overexpression enhanced ISGylation as well as IFN-β production, and conferred antiviral activity against vesicular stomatitis virus and Newcastle disease virus, which indicated that Herc6 is likely the functional antiviral factor in mouse cells (Oudshoorn and others 2012).

Here, we established the Herc6 null mice to study their role in protein ISGylation *in vivo*. Herc6 knockout mice lacked protein ISGylation. Herc6-deficient primary MEFs and bone marrow-derived macrophages (BMDM) lost the capacity to conjugate ISG15 to a broad group of proteins. These analyses with our newly generated Herc6 knockout mice confirmed the previous finding in the *in vitro* system that Herc6 is the major ISG15 E3 ligase in mice. Furthermore, we examined STAT1 phospharylation on IFN-β treatment, production of IFN-β and IL-6 after SV infection, or double-stranded RNA poly I:C treatment of WT and Herc6$^{-/-}$ BMDM. No significant difference was detected. In addition, the virus titers of VSV in WT and Herc6$^{-/-}$ MEFs were similar. These results indicate that Herc6-mediated protein ISGylation has no obvious effect on IFN signaling and antiviral activity against SV and VSV under current experimental conditions. As a critical different phenotype from ISG15 E1 Ube1L knockout mice that also lack protein ISGylation, male Herc6-deficient mice showed severe seminal vesicle hypertrophy. This finding suggests that Herc6 has a role in regulating sperm sac morphology, which is independent of protein ISGylation.

Materials and Methods

Generation of Herc6 knockout mice

The *Herc6* mutant mice (accession No. CDB0585K; www.cdb.riken.jp/arg/mutant%20mice%20list.html) were generated by gene targeting in TT2 embryonic stem (ES) cells (Yagi and others 1993), as previously described (www.cdb.riken.jp/arg/Methods.html). Two *Herc6* mutant mouse strains (line 1, #29 and line 2, #51) were established from independent homologous recombinant ES cells, and no difference in phenotype was apparent between them. In this study, all of the experiments were carried out with line 1 (#29) mice.

Animal studies

CBA/C57BL6 Mix background Herc6 KO (4 times backcrossed) mice and C57BL6 pure background WT and Herc6 KO mice were maintained at Kobe BM laboratory (Oriental Bio Service, Inc.). C57BL6 pure background WT and UBE1L KO mice were maintained at UCSD Moores cancer center. Animal studies in Kobe BM laboratory were properly conducted in accordance with regulations regarding animal experiments in Japan. Animal experiments in UCSD Moores cancer center were performed in accordance with NIH policies on the use of laboratory animals and approved by the Animal Research Committee of the Office for the Protection of Research Subjects at the University of California, San Diego.

Southern blotting and PCR genotyping

Southern blots were performed using a radioactive label or DIG label (Roche) methods according to the manufacturer's protocols. The probe for Southern blotting was amplified using primers as follows: Fw (5′-TGA AGACAG ACA AGG TGG AAT AAC TTG ATA-3′), Rev (5′-CAG CTG CAG TAC CAC AGG TGA TGT GGT ACT-3′). The genotyping of mice was routinely performed with tail by PCR using a mixture of 3 primers after overnight treatment with proteinase K in PCR buffer. The sizes of the PCR products are WT allele (258 bp) and mutant allele (787 bp). The PCR primers were as follows: P1 (5′-ACA GGA TGT GAT AGG CTG CAT GTG AAA G-3′) and P3 (5′-AAA CAC CTA GTT CCC GAG GCT GTG AAC T-3′) for the *Herc6* WT allele; P2 (5′-ATC AGG ATG ATC TGG ACG AAG AGC ATC A-3′) and P3 for the *Neo* gene. The PCR conditions were 95°C for 2 min, 40 cycles of 95°C for 30 s, 55°C for 30 s, and 72°C for 1 min, followed by 72°C for 10 min.

Cell culture and transfection

MEFs were prepared from E12.5 embryos and grown in Dulbecco's modified Eagle medium supplemented with glutamine, penicillin/streptomycin, and 10% fetal bovine serum (FBS). BMDM were cultured in RPMI1640 medium supplemented with glutamine, penicillin/streptomycin, 10% FBS, and macrophage colony-stimulating factor. For the knockdown analysis, siRNA was transfected using Lipofectamine 2000 (Invitrogen) according to the manufacturer's instruction. At 72 h after the siRNA transfection, cell lysates were prepared for examination.

Antibodies and reagents

Anti-mouse Herc6 polyclonal antibodies were generated in rabbits by using the mouse Herc6 recombinant protein that was bacterially produced using GST (6P-1) mHerc6 652-1003aa. Antibodies against STAT1, p-STAT1 (Y701), and ISG15 (#2743) were purchased from Cell Signaling. For the detection of protein ISGylation in liver and spleen tissue samples of WT and Herc6 knockout mice with or without poly I:C injection, and BMDM samples of WT and Herc6 knockout mice with or without IFN-β treatment, we used Dong-Er Zhang Lab's anti-mouse ISG15 antibody. Anti-α-tubulin (Sigma) and actin were acquired from Oncogene Research Products. Poly I:C was purchased from Amersham. Mouse IFN-β was purchased from PBL. Sendai virus (Z strain) and VSV were kindly provided by Dr. Masato Nakanishi (Research center for stem cell engineering, AIST, Japan).

Knockdown

For knockdown of Herc6, the following siRNAs were used:

si-Herc6-1: 5′-gaaauaagcuuuaugccuauu-3′ (B-Bridge International, Inc.)

si-Herc6-2: 5′-ggaacaaaguuaaagaacauu-3′ (B-Bridge International, Inc.)

si-Herc6-3: 5′-ccuacagaaugaaggaauauu-3′ (B-Bridge International, Inc.)

Control siRNA (si-GFP); 5′-acuuguacagcucguccauuu-3′ (B-Bridge International, Inc.)

Western blotting

Western blotting was conducted as previously described (Arimoto and others 2010). All samples were denatured in 1× sample buffer [50 mM Tris-HCl (pH 6.8), 2% sodium dodecyl sulfate (SDS), 2-mercaptethanol, 10% glycerol, and 1% bromophenol blue] for 5 min at 100°C. Cells were lysed in RIPA buffer composed of 25 mM Tris-HCl (pH 8.0), 150 mM NaCl, 1 mM EDTA, 1 mM dithiothreitol, 0.1% SDS, 1% Nonidet P-40, and 0.5% sodium deoxycholate. The cell lysates were centrifuged (10,000 *g*) at 4°C for 5 min. All lysis buffer in this study contains proteinase and phosphatase inhibitors (Roche). For the quantification, the Fujifilm Multi-gauge V3.0 was used.

Enzyme-linked immunosorbent assay

Culture media were collected and analyzed for IFN-β and IL-6 production by using enzyme-linked immunosorbent assays (ELISAs). ELISA kits for mouse IFN-β and IL-6 were purchased from PBL Biomedical Laboratories.

TCID50 assay

50% tissue culture infectious dose (TCID50) assay was conducted as previously described (Arimoto and others 2010). Approximate viral titers were calculated by TCID50 assay. Results of this assay are well in accordance with those of the general plaque assay. After 12 h VSV infection,

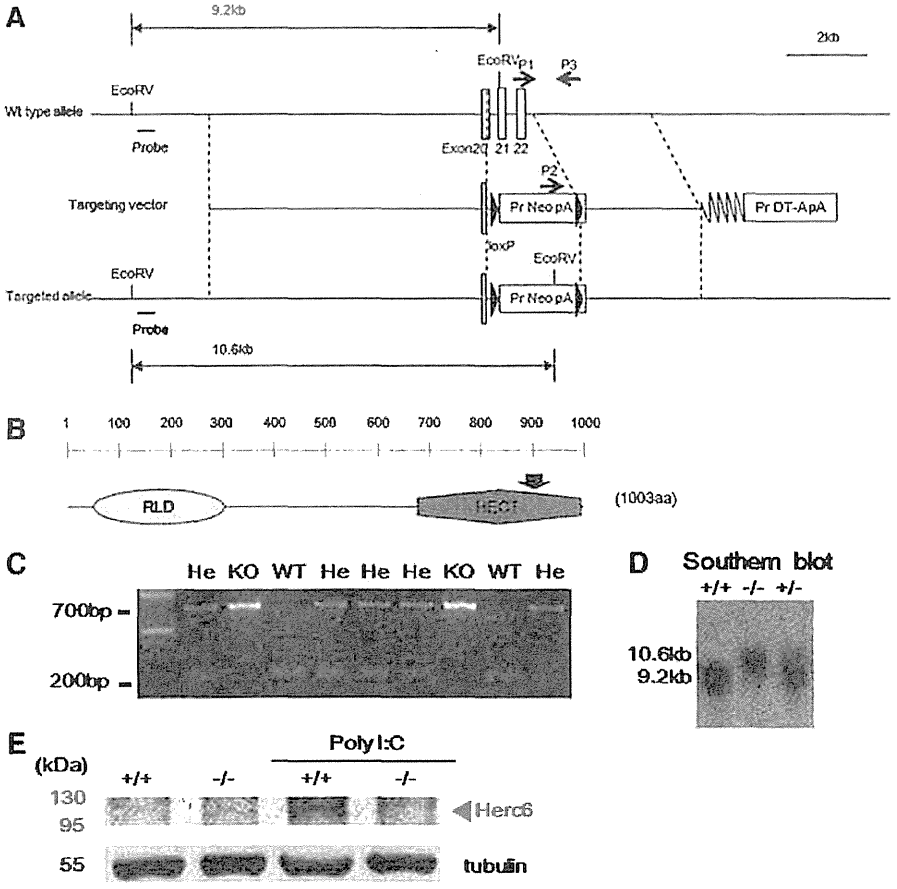

FIG. 1. Generation of Herc6 knockout mice. **(A)** Schematics of Herc6 knockout strategy. **(B)** Schematic diagram of Herc6 protein and the target deletion region is indicated with an *arrow*. **(C)** PCR genotyping of mouse tail DNA. **(D)** Southern blot analysis of mouse tail DNA. **(E)** Western blot analysis of protein ISGylation. Twenty-four hours after poly I:C injection, spleens were harvested. Herc6 protein was detected in the spleen extracts from WT mice, but not from Herc6 knockout mice by Western blotting using anti-mouse Herc6 polyclonal antibody. WT, wild type; He, heterozygous; KO, knockout.

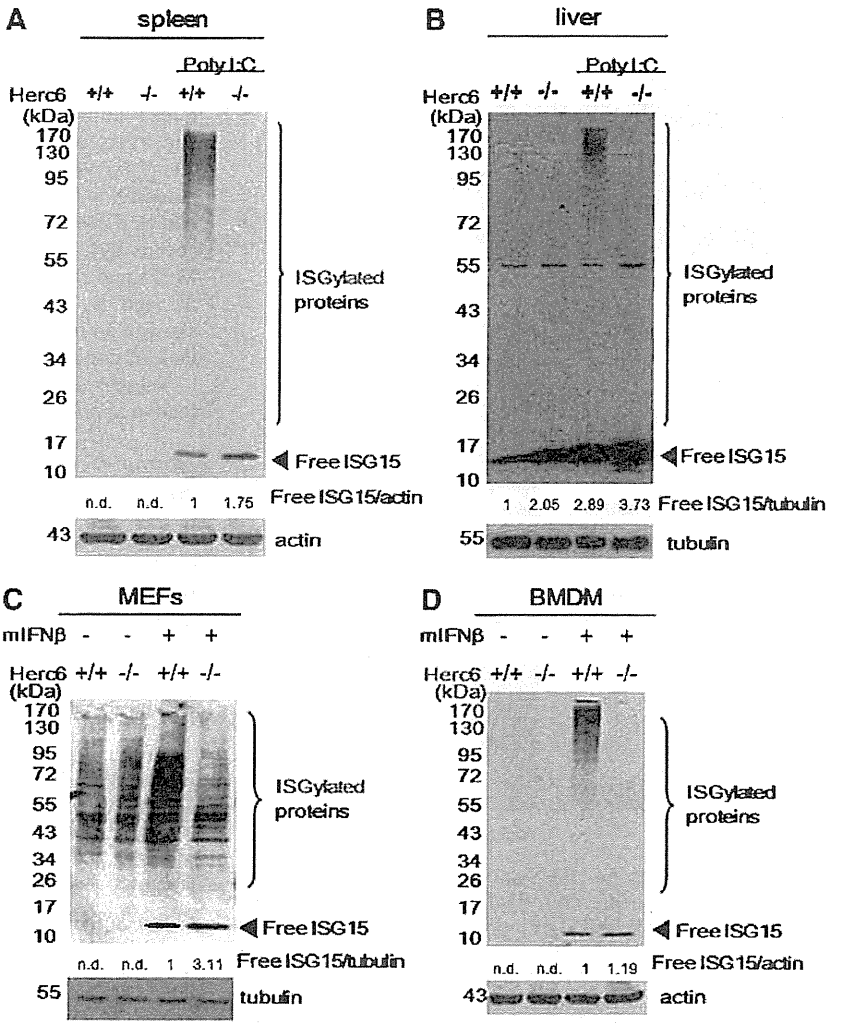

FIG. 2. Analysis of protein ISGylation in Herc6 knockout mice. (**A**, **B**) Twenty-four hours after PBS or poly I:C injection, spleens and livers were harvested, and ISG15 conjugated protein was detected by Western blotting using anti-mouse ISG15 antibody (Dong-Er Zhang Lab). (**C**) Mouse embryonic primary fibroblasts from WT and Herc6 knockout mice were treated with mock or 500 U/mL of mIFN-β. Twenty-four hours after treatment, cells were harvested and subjected to Western blotting using anti-ISG15 antibody (CST#2743), the information of which should be in M&M. (**D**) BMDM from wild-type and Herc6 knockout mice were treated with mock or 100 U/mL of mIFN-β as indicated. Twenty-four hours after treatment, cells were harvested and subjected to Western blotting using anti-mouse ISG15 antibody (Dong-Er Zhang Lab). The levels of free ISG15 were quantified as indicated. n.d. means not detectable. BMDM, bone marrow-derived macrophages; IFN, interferon.

the culture medium was diluted 3×10^4 times and then added to the first line of a 96-well plate with 50 μL medium containing 293T cells, making a serial 3-fold dilution. At 1–2 days after infection, more than 50% cell alterations in each dilution step was analyzed with the following formula: $TCID50 = (\text{rate of dilution at first line}) \times (\text{dilution rate})^{\Sigma - 0.5}$, where Σ = the number of wells observed with more than 50% cell alteration in each dilution step/sample sum.

Histology

Whole body was fixed by 10% formaldehyde solution, and tissues were paraffin embedded into OCT compound (Tissue-Tek). For histochemical analysis, paraffin sections were stained with H&E according to standard protocols.

Results

Disruption of the mouse Herc6 gene

In line with the previous report using L929 cells and siRNA against Herc6 (Oudshoorn and others 2012), we observed the reduction of ISGylation in Herc6 knockdown primary MEFs after IFN treatment (Supplementary Fig. S1; Supplementary Data are available online at www.liebertpub.com/jir). To investigate the role of protein ISGylation by Herc6 *in vivo*, we generated Herc6 knockout mice. For the disruption of the Herc6 gene, we added 2 *loxP* sites to exon 20 and the intron after exon 22 (Fig. 1A). This target region is related to C-terminal HECT domain of Herc6 protein (Fig. 1B). This construct also contains the bacterial neomycin gene as a selection marker in the Herc6 gene. Chimeric mice were produced by an injection of 2 independent clones of heterozygous ES cells into CBA blastocyst-stage embryos, and germ line transmission was determined by breeding with WT C57BL6 mice. We further backcrossed $Herc6^{+/-}$ mice with C57BL6 mice 4 times and 8 times to generate CBA/C57BL6 mix background and C57BL6 background Herc6 null mice, respectively. Mice were genotyped by PCR (Fig. 1C), and confirmed by Southern blot analysis (Fig. 1D). To confirm that Herc6 is no longer expressed in the knockout mice, spleens of WT and $Herc6^{-/-}$ mice that were with or without poly I:C injection were homogenized and subjected to Western blot. Herc6 protein was identified in poly I:C injected WT, but not in Herc6 knockout mouse (Fig. 1E).

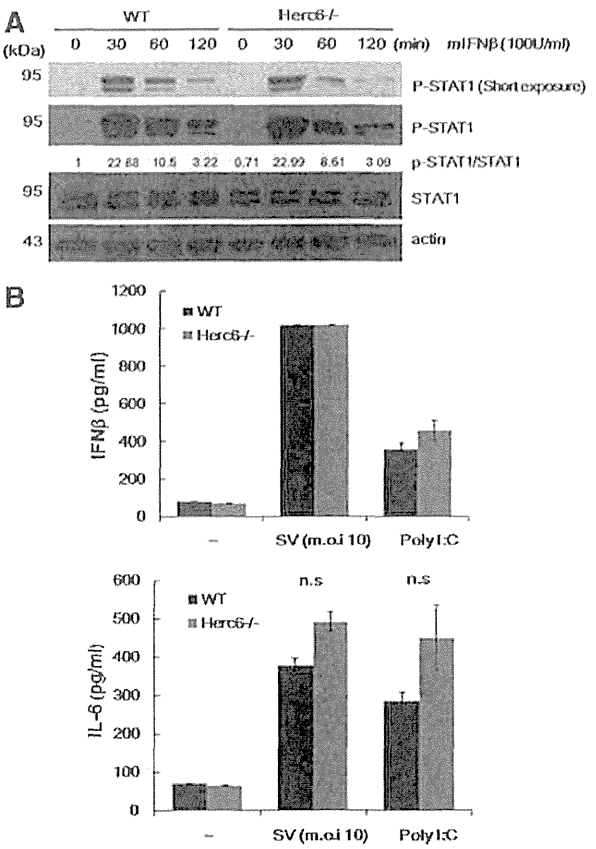

FIG. 3. Analysis of IFN and inflammatory response in Herc6 knockout cells. (**A**) BMDM from WT and Herc6 knockout mice were cultured in the presence of 100 U/mL of mIFN-β for the indicated time periods. Cells were harvested and subjected to Western blotting against pSTAT1, STAT1, and actin. The ratio of p-STAT1/total-STAT1 was also quantified as indicated. (**B**) Macrophages from WT and Herc6 knockout mice were treated with mock, SV at m.o.i. 10, or poly I:C 10 μg/mL. Twenty-four hours after treatment, cell culture media were harvested and subjected to ELISA for mIFN-β (*upper*) or mIL-6 (*bottom*). ELISA, enzyme-linked immunosorbent assay; m.o.i., multiplicity of infection; SV, Sendai virus.

Defective protein ISGylation in Herc6 knockout mice

To determine whether lack of Herc6 correlated with decreased ISGylation *in vivo*, we injected WT and knockout mice with PBS or poly I:C. Twenty-four hours later, spleens and livers were harvested, and protein ISGylation was detected by Western blotting. Protein ISGylation was readily detected in the liver and spleen from WT but was barely detected from Herc6 knockout mice (Fig. 2A and B, respectively). Similar results were observed in IFN-β-treated MEFs and BMDM from WT and Herc6 knockout mice (Fig. 2C and D, respectively). Herc6-deficient tissues or cells showed an increased amount of free ISG15 as a result of the lack of conjugation (Fig. 2A–D).

These results indicate that Herc6 knockout mice are defective in protein ISGylation but not in free ISG15 expression.

Normal IFN responses of Herc6-deficient cells and mice

A previous report has shown that human HERC5 positively regulates the IFN-β promoter via enhancing IRF3 function and so confers antiviral activity (Shi and others 2010). In addition, mouse Herc6 also enhanced IFN-β promoter activity similar to its human Herc5 counterpart (Oudshoorn and others 2012). To explore whether Herc6 regulates IFN signal transduction, we examined the IFN-response of Herc6-deficient cells. Macrophages derived from bone marrow cells of WT and Herc6 knockout mice were cultured *in vitro* and treated with 100 U/mL of IFN-β, and STAT1 phosphorylation was detected as an indication of the activation of the signaling pathway. Increased phosphorylation of STAT1 on IFN treatment was observed. However, there was no difference of STAT1 phosphorylation between WT and Herc6-deficient cells (Fig. 3A).

To investigate whether the mouse Herc6 enhances an innate immune signal, we examined the IFN-β and IL-6 production in WT and Herc6$^{-/-}$ MEFs on Sendai virus infection and poly I:C stimulation. No significant differences in WT and Herc6 cells were observed (Fig. 3B top and bottom, respectively). Although it was not significant, a modest increase of IL-6 production in Herc6$^{-/-}$ MEFs with SV infection or poly I:C stimulation was observed (Fig. 3B bottom). This should be investigated with greater detail in the future.

Since lipopolysaccharide (LPS) activates the expression of these genes via the IFN signaling pathway, we also examined the peripheral blood cell count and other blood parameters.

TABLE 1. BLOOD ANALYSIS WITH OR WITHOUT LPS (15 mg/kg BODY WEIGHT) INJECTION

	WBC ($10^3/\mu L$)	*RBC* ($10^3/\mu L$)	*Hb (g/dL)*	*Ht (%)*	*MCV (fl)*	*MCH (pg/cell)*	*MCHC (g/dL)*	*PLT* ($10^3/\mu L$)
Mock								
WT ($n=3$)	7.7±1.4	8.0±0.2	12.3±0.1	38.6±1.2	48±0.2	15.4±0.3	32.0±0.8	107.9±34.7
KO ($n=2$)	6.5±0.3	6.8±0.2	12±0.9	32.9±8.2	48.2±2.4	18.1±4.3	37.3±7.2	118.9±13.4
LPS								
WT ($n=5$)	3.0±0.5	8.1±0.2	12.7±0.1	39.9±1.3	48.9±0.4	15.8±0.3	31.9±0.7	346.0±10.2
KO ($n=5$)	3.6±0.8	8.1±0.4	13.0±0.8	40.8±2.1	50.1±0.3	16.0±0.3	31.8±0.7	301.0±9.51

Blood samples were collected via retro-orbital bleeding from wild-type and Herc6 knockout mice at 1 day after with or without LPS (15 mg/kg body weight) injections. Values are means±standard deviation.

WBC, white blood corpuscles; RBC, red blood corpuscles; Hb, hemoglobin; Ht, hematocrit; MCV, mean corpuscular volume; MCH, mean corpuscular hemoglobin; MCHC, mean corpuscular hemoglobin concentration; PLT, platelet; LPS, lipopolysaccharide; WT, wild type.

However, no significant differences were observed between WT and Herc6 knockout mice with or without LPS stimulation (Table 1).

In summary, Herc6-deficient cells do not show any detectable differences from WT cells in their responses to IFN-related treatments.

Deletion of Herc6 did not affect the antiviral response against VSV infection

Besides the IFN response (Shi and others 2010), a recent report indicated that Herc5 mainly conjugates ISG15 to newly synthesized proteins in tissue culture and may by this mechanism largely target *de novo* synthesized viral proteins during infection (Durfee and others 2010).

To investigate whether Herc6 affects the proliferation of virus, we examined the consequences of reduction of protein ISGylation on the antiviral effects of IFN in MEFs. Treatment

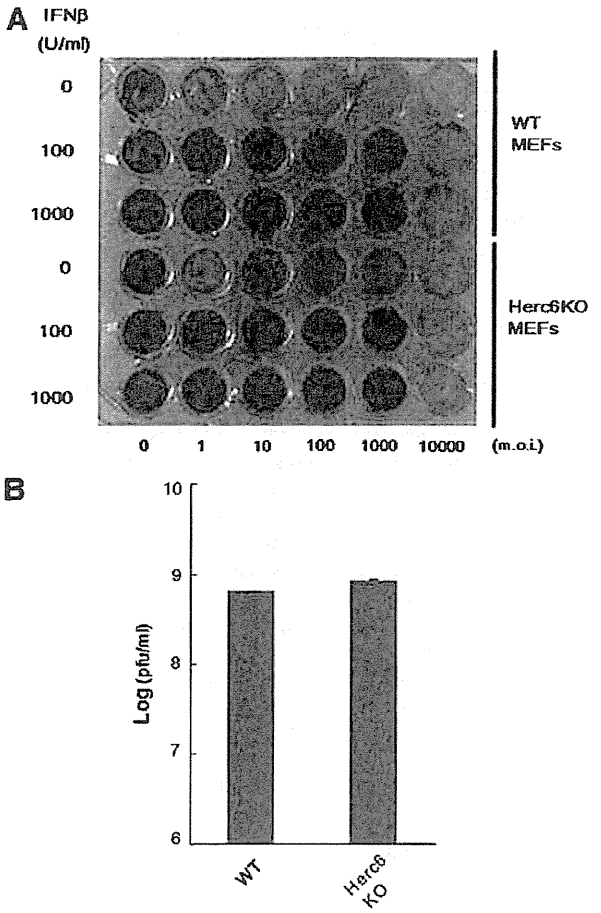

FIG. 4. VSV protection assay. (A) WT and Herc6 knockout MEFs were left untreated or treated with 100 or 1,000 U/mL of IFN-β for 24 h, followed by VSV infection at m.o.i. $0–10^4$ per well for an additional 24 h. Cell viability was assessed by crystal *violet* staining. (B) The VSV (m.o.i. 0.1) was infected with WT and Herc6 knockout MEFs. At 12 h after infection, virus titer was measured according to TCID50 protocol. Data are mean ± SD ($n = 3$). MEFs, mouse embryonic fibroblast cells; TCID50, 50% tissue culture infectious dose; VSV, vesicular stomatitis virus.

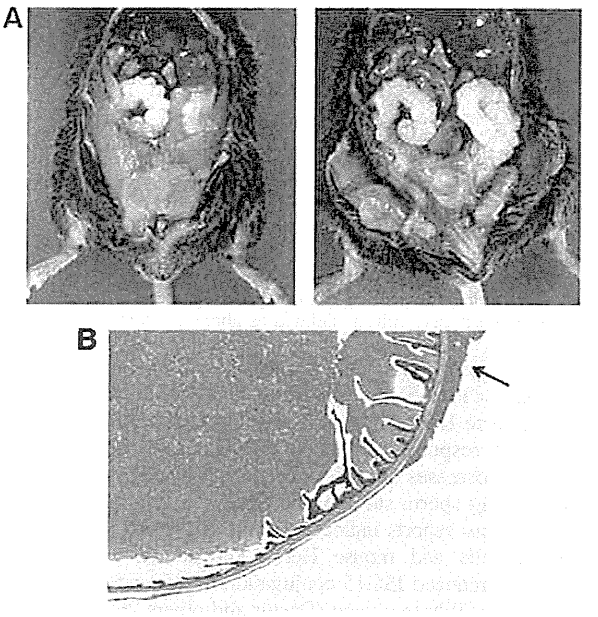

FIG. 5. The phenotype of Herc6 knockout mice. (A) The representative enlarged seminal vesicle in Herc6 knockout mouse (30 weeks, mix background). *Right panel* shows incision of the peritoneum of the left mouse. (B) H&E staining for the seminal vesicle of Herc6 knockout mouse. *Arrow* shows epithelial hyperplasia of seminal vesicle.

with increasing concentrations of IFN-β correlated positively with the antiviral stage of both WT and Herc6 knockout MEFs on infection with VSV, with no detectable differences in the response between the 2 genotypes (Fig. 4A). In addition, there was no significant difference of viral titer between WT and Herc6 knockout MEFs after infection with VSV (Fig. 4B). These experiments demonstrate that protein ISGylation via Herc6 in mice is not involved in the antiviral response against VSV.

Male Herc6 null mice showed hypertrophy of seminal vesicle

During the experiments, we noticed that mix-background Herc6 knockout male mice began showing abdominal distension at 28 weeks. Severe enlargement seminal vesicles were observed in Herc6 knockout mice (Fig. 5A). However, only slight epithelial hyperplasia with cystic dilatation of seminal vesicles was observed in Herc6 knockout mice (Fig. 5B), suggesting that the enlargement of seminal vesicles was from increased seminal fluid. Glandular hypoplasia and benign hypertrophy of the prostate, which are commonly found in elderly men, were not observed in Herc6 knockout mice (data not shown). Further examination using C57BL6 background mice showed a higher frequency of enlargement of seminal vesicles in Herc6 knockout mice compared with WT or UBE1L knockout mice (Table 2 and Supplementary Fig. S2). These results demonstrate that mouse Herc6 has an ISG15-independent function in regulating the seminal component.

Discussion

In this article, we described the generation and analysis of the first Herc6 knockout mouse model. The results of our

TABLE 2. ANALYSIS OF SEMINAL VESICLE OF WT, UBE1L$^{-/-}$, AND HERC6$^{-/-}$, MICE

Background	*Genotype*	*Population of hypertrophied seminal vesicle*		
		30 weeks	50 weeks	~90 weeks
Mix (CBA/C57BL6)	Herc6$^{-/-}$ ($n=5$)	2	4	
C57	WT ($n=10$)		0	2
	UBE1L$^{-/-}$ ($n=5$)		0	0
	Herc6$^{-/-}$ ($n=9$)		1[a]	8

[a]One-side anomalistic seminal hypertrophy.
Seminal hypertrophy is defined as above at least 0.04 g seminal vesicle/g body weight.

studies demonstrate that (1) Mouse Herc6 is the major E3 ligase for ISG15 conjugation *in vivo*. (2) ISG15 conjugation via mouse Herc6 does not affect type I IFN response and antiviral response against SV and VSV infection. (3) Mouse Herc6 possesses an ISG15 conjugation-independent role in regulating sperm sac morphology.

Previous reports indicate that human Herc5 knockdown in 293T cells and mouse Herc6 knockdown in L929 cells showed reduced ISG15 conjugation to a broad group of proteins after IFN treatment (Dastur and others 2006; Wong and others 2006; Oudshoorn and others 2012). In line with this result, the level of ISG15 conjugation in tissues of Herc6-deficient mice showed substantial reduction compared with that of WT mice after poly I:C injection. These findings clearly indicate that Herc6 is the major mouse ISG15 E3 ligases *in vivo*. Furthermore, our report supports that humans and mice developed different Herc proteins to facilitate global ISG15 conjugation during evolution.

A recent report indicates that HERC5 is mainly associated with poly-ribosome, and ISGylation targets newly synthesized proteins in human tissue culture (Durfee and others 2010). Furthermore, in this same report, the authors showed that HPV16 L1 capsid protein was ISGylated and this modification inhibited HPV pseudovirus production in transfection experiments (Durfee and others 2010). In addition, previous reports showed that antiviral effects exerted by human HERC5 (Shi and others 2010) are shared by Herc6 in mouse cells (Oudshoorn and others 2012). ISG15-activating enzyme Ube1L knockout mice also showed no protein ISGylation and no difference in IFN responses and anti-VSV and LCMV defense (Osiak and others 2005; Kim and others 2006). However, further studies of Ube1L knockout mice revealed a critical role of Ube1L in control of influenza B virus infection (Lai and others 2009). These discrepancies of revealed functions of protein ISGylation are likely due to the differences in species (humans and mice), lines, and viruses, and *in vitro* versus *in vivo* experiments. These questions need to be addressed in the future.

Herc6 null mice showed hypertrophy of seminal vesicles in both CBA/C56BL6 mixed background and C57BL6 background. However, Ube1L$^{-/-}$ mice did not show similarly enlarged sperm sacs although protein ISGylation is lost in both Herc6 and Ube1L knockout mice (Kim and others 2006). This difference suggests that mouse Herc6 has an ISG15-independent function in seminal fluid production during aging. However, the phenotype of Herc6$^{-/-}$ ISG15$^{-/-}$ also should be investigated in the future to examine whether this seminal hypertrophy is truly Herc6 dependent and ISG15 independent. Since mouse Herc6 belongs to the Herc family of ubiquitin E3 ligases, it is possible that ISG15 conjugation is regulated by the ISG15 E3 ligase activity of Herc6, and seminal component secretion is regulated by its ubiquitin E3 ligase activity. Human Herc5 may have evolved to exclusively function as an ISG15 E3 ligase, while human Herc6 may function as a ubiquitin E3 ligase that is involved in the seminal component secretion.

While we could not see the difference in male fertility of Herc6 knockout mice (~35 weeks) (data not shown), we cannot rule out this possibility because it could be affected by the conditions associated with older age.

The function of seminal fluid is largely unknown except for the involvement of normal conception. Interestingly, it has recently been reported that paternal seminal fluid composition affects the epigenome of male offspring and that its impact on the periconception environment involves not only sperm protection but also indirect effects on various female factors regulating embryo development, which suggests that offspring of Herc6 null mice may have interesting epigenomic changes by the hypertrophied seminal vesicles of Herc6 male mice (Bromfield and others 2014). Future studies using this mouse model may facilitate to address this question.

In humans, symptoms of enlarged seminal vesicles are frequently seen in patients with ejaculatory duct obstructions (EDO) (Pryor and Hendry 1991). EDO is a congenital or acquired pathological condition that is characterized by the obstruction of one or both ejaculatory ducts, and causes 1%–5% of male infertility (Philip and others 2007). In addition to the congenital form that is often caused by cysts of the müllerian duct, the obstruction can be acquired due to an inflammation caused by chlamydia, prostatitis, tuberculosis of the prostate, and other pathogens (Philip and others 2007). However, in many patients, there is no history of inflammation and the underlying cause simply remains unknown (Philip and others 2007). The finding that the suppression of Herc6 caused the hypertrophied seminal vesicles in this report may be involved in the acquired enlarged seminal vesicle symptoms, and this should be investigated in the future.

Acknowledgments

The authors thank all lab members for helpful discussion. They especially thank Dr. Kentson Lam (School of Medicine, University of California San Diego) and Samuel Stoner (Moores Cancer Center, University of California San Diego) for discussion and a critical reading of this article. They also thank Shuichiro Ogawa (Kyoto University) for several experiments and discussion. This study was supported by Grants-in-Aid for Scientific Research from the Ministry of Education, Culture, Sports, Science, and Technology (22114004 & 22249012), funding from National Institutes of Health USA (R01CA177305 and R01HL091549), and

JSPS KAKENHI Grant (No. 10J00577); Kei-ichiro Arimoto is a JSPS Postdoctoral Fellow for Research Abroad.

Author Disclosure Statement

There is no financial interest to disclose.

References

Arimoto K, Funami K, Saeki Y, Tanaka K, Okawa K, Takeuchi O, Akira S, Murakami Y, Shimotohno K. 2010. Polyubiquitin conjugation to NEMO by triparite motif protein 23 (TRIM23) is critical in antiviral defense. Proc Natl Acad Sci U S A 107(36):15856–15861.

Bedford L, Lowe J, Dick LR, Mayer RJ, Brownell JE. 2011. Ubiquitin-like protein conjugation and the ubiquitin-proteasome system as drug targets. Nature reviews. Drug Discov 10(1):29–46.

Bromfield JJ, Schjenken JE, Chin PY, Care AS, Jasper MJ, Robertson SA. 2014. Maternal tract factors contribute to paternal seminal fluid impact on metabolic phenotype in offspring. Proc Natl Acad Sci U S A 111(6):2200–2205.

Burkart C, Arimoto K, Tang T, Cong X, Xiao N, Liu YC, Kotenko SV, Ellies LG, Zhang DE. 2013. Usp18 deficient mammary epithelial cells create an antitumour environment driven by hypersensitivity to IFN-lambda and elevated secretion of Cxcl10. EMBO Mol Med 5(7):967–982.

Dastur A, Beaudenon S, Kelley M, Krug RM, Huibregtse JM. 2006. Herc5, an interferon-induced HECT E3 enzyme, is required for conjugation of ISG15 in human cells. J Biol Chem 281(7):4334–4338.

Durfee LA, Lyon N, Seo K, Huibregtse JM. 2010. The ISG15 conjugation system broadly targets newly synthesized proteins: implications for the antiviral function of ISG15. Mol Cell 38(5):722–732.

Guerra S, Caceres A, Knobeloch KP, Horak I, Esteban M. 2008. Vaccinia virus E3 protein prevents the antiviral action of ISG15. PLoS Pathog 4(7):e1000096.

Hochrainer K, Mayer H, Baranyi U, Binder B, Lipp J, Kroismayr R. 2005. The human HERC family of ubiquitin ligases: novel members, genomic organization, expression profiling, and evolutionary aspects. Genomics 85(2):153–164.

Hsiang TY, Zhao C, Krug RM. 2009. Interferon-induced ISG15 conjugation inhibits influenza A virus gene expression and replication in human cells. J Virol 83(12):5971–5977.

Hsiao NW, Chen JW, Yang TC, Orloff GM, Wu YY, Lai CH, Lan YC, Lin CW. 2010. ISG15 over-expression inhibits replication of the Japanese encephalitis virus in human medulloblastoma cells. Antiviral Res 85(3):504–511.

Kim KI, Giannakopoulos NV, Virgin HW, Zhang DE. 2004. Interferon-inducible ubiquitin E2, Ubc8, is a conjugating enzyme for protein ISGylation. Mol Cell Biol 24(21):9592–9600.

Kim KI, Yan M, Malakhova O, Luo JK, Shen MF, Zou W, de la Torre JC, Zhang DE. 2006. Ube1L and protein ISGylation are not essential for alpha/beta interferon signaling. Mol Cell Biol 26(2):472–479.

Lai C, Struckhoff JJ, Schneider J, Martinez-Sobrido L, Wolff T, Garcia-Sastre A, Zhang DE, Lenschow DJ. 2009. Mice lacking the ISG15 E1 enzyme UbE1L demonstrate increased susceptibility to both mouse-adapted and non-mouse-adapted influenza B virus infection. J Virol 83(2):1147–1151.

Lenschow DJ. 2010. Antiviral properties of ISG15. Viruses 2(10):2154–2168.

Lenschow DJ, Giannakopoulos NV, Gunn LJ, Johnston C, O'Guin AK, Schmidt RE, Levine B, Virgin HWt. 2005. Identification of interferon-stimulated gene 15 as an antiviral molecule during Sindbis virus infection *in vivo*. J Virol 79(22):13974–13983.

Lenschow DJ, Lai C, Frias-Staheli N, Giannakopoulos NV, Lutz A, Wolff T, Osiak A, Levine B, Schmidt RE, Garcia-Sastre A, Leib DA, Pekosz A, Knobeloch KP, Horak I, Virgin HWt. 2007. IFN-stimulated gene 15 functions as a critical antiviral molecule against influenza, herpes, and Sindbis viruses. Proc Natl Acad Sci U S A 104(4):1371–1376.

Malakhova OA, Zhang DE. 2008. ISG15 inhibits Nedd4 ubiquitin E3 activity and enhances the innate antiviral response. J Biol Chem 283(14):8783–8787.

Okumura A, Lu G, Pitha-Rowe I, Pitha PM. 2006. Innate antiviral response targets HIV-1 release by the induction of ubiquitin-like protein ISG15. Proc Natl Acad Sci U S A 103(5):1440–1445.

Okumura A, Pitha PM, Harty RN. 2008. ISG15 inhibits Ebola VP40 VLP budding in an L-domain-dependent manner by blocking Nedd4 ligase activity. Proc Natl Acad Sci U S A 105(10):3974–3979.

Osiak A, Utermohlen O, Niendorf S, Horak I, Knobeloch KP. 2005. ISG15, an interferon-stimulated ubiquitin-like protein, is not essential for STAT1 signaling and responses against vesicular stomatitis and lymphocytic choriomeningitis virus. Mol Cell Biol 25(15):6338–6345.

Oudshoorn D, van Boheemen S, Sanchez-Aparicio MT, Rajsbaum R, Garcia-Sastre A, Versteeg GA. 2012. HERC6 is the main E3 ligase for global ISG15 conjugation in mouse cells. PLoS One 7(1):e29870.

Park JM, Yang SW, Yu KR, Ka SH, Lee SW, Seol JH, Jeon YJ, Chung CH. 2014. Modification of PCNA by ISG15 plays a crucial role in termination of error-prone translesion DNA synthesis. Mol Cell 54(4):626–638.

Philip J, Manikandan R, Lamb GH, Desmond AD. 2007. Ejaculatory-duct calculus causing secondary obstruction and infertility. Fertil Steril 88(3):706 e9–e11.

Pincetic A, Kuang Z, Seo EJ, Leis J. 2010. The interferon-induced gene ISG15 blocks retrovirus release from cells late in the budding process. J Virol 84(9):4725–4736.

Pryor JP, Hendry WF. 1991. Ejaculatory duct obstruction in subfertile males: analysis of 87 patients. Fertil Steril 56(4):725–730.

Shi HX, Yang K, Liu X, Liu XY, Wei B, Shan YF, Zhu LH, Wang C. 2010. Positive regulation of interferon regulatory factor 3 activation by Herc5 via ISG15 modification. Mol Cell Biol 30(10):2424–2436.

Wong JJ, Pung YF, Sze NS, Chin KC. 2006. HERC5 is an IFN-induced HECT-type E3 protein ligase that mediates type I IFN-induced ISGylation of protein targets. Proc Natl Acad Sci U S A 103(28):10735–10740.

Yagi T, Tokunaga T, Furuta Y, Nada S, Yoshida M, Tsukada T, Saga Y, Takeda N, Ikawa Y, Aizawa S. 1993. A novel ES cell line, TT2, with high germline-differentiating potency. Anal Biochem 214(1):70–76.

Yuan W, Krug RM. 2001. Influenza B virus NS1 protein inhibits conjugation of the interferon (IFN)-induced ubiquitin-like ISG15 protein. EMBO J 20(3):362–371.

Address correspondence to:
Dr. Kei-ichiro Arimoto
Moores UCSD Cancer Center
University of California, San Diego
3855 Health Sciences Drive
La Jolla, CA 92093

E-mail: karimoto@ucsd.edu

Received 11 July 2014/Accepted 29 September 2014

PLOS ONE

Comparison of Hepatocellular Carcinoma miRNA Expression Profiling as Evaluated by Next Generation Sequencing and Microarray

Yoshiki Murakami[1]*, Toshihito Tanahashi[2,3], Rina Okada[3], Hidenori Toyoda[4], Takashi Kumada[4], Masaru Enomoto[1], Akihiro Tamori[1], Norifumi Kawada[1], Y-h Taguchi[5], Takeshi Azuma[3]

1 Department of Hepatology, Osaka City University Graduate School of Medicine, Osaka, Japan, 2 Department of Medical Pharmaceutics, Kobe Pharmaceutical University, Kobe, Japan, 3 Division of Gastroenterology, Department of Internal Medicine, Kobe University Graduate School of Medicine, Kobe, Japan, 4 Department of Gastroenterology, Ogaki Municipal Hospital, Ogaki, Japan, 5 Department of Physics, Chuo University, Tokyo, Japan

Abstract

MicroRNA (miRNA) expression profiling has proven useful in diagnosing and understanding the development and progression of several diseases. Microarray is the standard method for analyzing miRNA expression profiles; however, it has several disadvantages, including its limited detection of miRNAs. In recent years, advances in genome sequencing have led to the development of next-generation sequencing (NGS) technologies, which significantly advance genome sequencing speed and discovery. In this study, we compared the expression profiles obtained by next generation sequencing (NGS) with the profiles created using microarray to assess if NGS could produce a more accurate and complete miRNA profile. Total RNA from 14 hepatocellular carcinoma tumors (HCC) and 6 matched non-tumor control tissues were sequenced with Illumina MiSeq 50-bp single-end reads. Micro RNA expression profiles were estimated using miRDeep2 software. As a comparison, miRNA expression profiles for 11 out of 14 HCCs were also established by microarray (Agilent human microRNA microarray). The average total sequencing exceeded 2.2 million reads per sample and of those reads, approximately 57% mapped to the human genome. The average correlation for miRNA expression between microarray and NGS and subtraction were 0.613 and 0.587, respectively, while miRNA expression between technical replicates was 0.976. The diagnostic accuracy of HCC, p-value, and AUC were 90.0%, 7.22×10^{-4}, and 0.92, respectively. In summary, NGS created an miRNA expression profile that was reproducible and comparable to that produced by microarray. Moreover, NGS discovered novel miRNAs that were otherwise undetectable by microarray. We believe that miRNA expression profiling by NGS can be a useful diagnostic tool applicable to multiple fields of medicine.

Citation: Murakami Y, Tanahashi T, Okada R, Toyoda H, Kumada T, et al. (2014) Comparison of Hepatocellular Carcinoma miRNA Expression Profiling as Evaluated by Next Generation Sequencing and Microarray. PLoS ONE 9(9): e106314. doi:10.1371/journal.pone.0106314

Editor: Max Costa, New York University School of Medicine, United States of America

Received March 10, 2014; **Accepted** July 29, 2014; **Published** September 12, 2014

Funding: The authors have no support or funding to report.

Competing Interests: The authors declare that they have no competing interests.

* Email: m2079633@med.osaka-cu.ac.jp

Introduction

MicroRNAs (miRNAs) are an abundant class of small (19–24 nt) and highly conserved, non-coding RNA. They act as post-transcriptional regulators of gene expression, altering mRNA transcription and translation by hybridizing to the untranslated regions (UTRs) of certain subsets of mRNAs [1] [2]. Since their initial discovery in *Caenorhabditis elegans* in 1993 [3], researchers have gained much insight into the prevalence of miRNAs in other species. The latest miRBase database (release 20) contains 1827 precursor miRNAs and 2578 mature miRNA products in *Homo sapiens* (http://www.mirbase.org/index.shtml).

Hepatocellular carcinoma (HCC) is a common cause of cancer-related deaths worldwide. There are more than 250,000 new HCC cases and an estimated 500,000–600,000 HCC deaths annually [4] [5]. The most frequent etiology of HCC is chronic hepatitis B and C (CHB, CHC), or alcoholic liver disease. Although recent advances in functional genomics provide a deeper understanding of viral associated hepatocarcinogenesis (review in [6]), the molecular pathogenesis of HCC remains unclear.

Altered miRNA expression has been observed in a large variety of HCC and a correlation has been found between miRNA expression and histological differentiation [7] [8]. For example, the expression level of miR-26 has been associated with hepatocarcinogenesis and response to interferon therapy [9]. Moreover recently, miR-122 expression was associated with hepatocarcinogenesis, liver homeostasis, and essential liver metabolism [10] [11]. miR-18 has also been highly associated with the occurrence and progression of different types of cancer [12] [13]. In other research, miRNA expression profiles were associated with vascular invasion, the levels of alpha-fetoprotein, and large tumor size [14].

To date, studies exploring the role of miRNAs in hepatocarcinogenesis have relied on microarrays to assay miRNA expression. Deep sequencing, a set of technologies that produce large amounts of sequence data from nucleic acid specimens, is rapidly replacing microarrays as the technology of choice for quantifying and annotating miRNAs [15] [16]. Deep sequencing has the superior ability to capture the scale and complexity of whole transcriptomes [17]. In particular, short read deep sequencing

(e.g., the Illumina MiSeq platform) is appropriate for miRNAs because a complete miRNA can be sequenced with a single read. While array design relies on prior knowledge of the miRNAs being investigated, deep sequencing allows for the discovery of novel miRNAs. Furthermore, microarray methods lack the dynamic range to detect and quantify low abundance transcripts, but deep sequencing can identify miRNAs that are expressed at levels that fall below microarray's detectable threshold. In addition, deep sequencing eliminates background problems that result from cross-hybridization in microarrays, thus facilitating interpretation of the signal and obviating the non-linear data manipulation steps required by microarrays. Therefore, the application of deep sequencing to miRNA profiling has the potential to uncover novel miRNAs and to detect expression of rare but functionally significant miRNAs. Recently, deep sequencing was used to analyze non-coding RNAs in HCC, by which miRNAs, PIWI-interacting RNA, and small nucleolar RNAs were identified [18].

In this study, we created miRNA expression profiles for HCC and non-tumorous tissue using NGS. We then compared the miRNA expression profiles obtained by NGA and microarray. Unlike previous studies, we sequenced un-pooled miRNA libraries to a previously unprecedented sequencing depth from multiple replicates and controls across multiple time-points, allowing us to explore the statistically significant temporal changes in miRNA expression in hepatocarcinogenesis.

Materials and Methods

Sample preparation

We isolated total RNA from 14 surgically resected HCC tumors and 6 matched adjacent non-tumor control tissues (Table 1). We confirmed that the 14 samples were accurately diagnosed as HCC by image diagnosis by CT and USTG and pathological findings. All patients or their guardians provided written informed consent, and Osaka City University and Ogaki Municipal Hospital approved all aspects of this study in accordance with the Helsinki Declaration.

RNA preparation, and miRNA deep sequencing and microarray

Total RNA from surgical resection was prepared using mirVana miRNA Isolation kit (Invitrogen), according to the manufacturer's instruction.

Total RNA, containing the small RNA fraction, was reverse transcribed into a cDNA library using the TruSeq Small RNA Sample Prep Kit (Illumina). Briefly, total RNA (1 μg per sample) was ligated overnight with adapters, reverse transcribed, RNase-treated, and PCR-amplified with unique barcode-labeled amplification primers. Then, size-selection was conducted on 6% native polyacrylamide gels. cDNA fragments between 145 and 160 bp corresponding to the miRNA populations were excised from the gel, then eluted and precipitated. The final cDNA pellet was air dried and resuspended in 10 μl of nuclease-free water. The quantity of cDNA in each final miRNA libraries was verified using Qubit fluorometer (Invitrogen). Equimoloar amounts for each final library were pooled at a final concentration of 2 nM cDNA. Barcoded templates were sequenced on a single flowcell of the Illumina MiSeq with 50-bp single-end reads. Eleven of 14 total HCC RNA samples were also assayed by microarray (Agilent human microRNA microarray release 14.0) (Table 1). Hybridization signals were detected with a DNA microarray scanner G2505B (Agilent Technologies) and the scanned images were analyzed using Agilent feature extraction software (v9.5.3.1). Raw data (gProcessedSignal) was normalized so that each expression had a mean of zero and a sample variance of one. The above processes were conducted with various packages and functions implemented in R {http://www.r-project.org}.

The sequence reads obtained in this study have been deposited in the DNA Data Bank of Japan Sequence Read Archive (http://www.ddbj.nig.ac.jp/index-e.html) under accession number DRA001067. All microarray data were deposited in NCBI's Gene Expression Omnibus and are accessible through GEO Series accession number GSE31164.

Bioinformatics

In order to extract the adaptor sequence from each short read obtained by NGS, fastx_clipper from the fastx toolkit {http://hannonlab.cshl.edu/fastx_toolkit/} was used. The adaptor trimmed short reads were then mapped to the human reference genome sequence hg19 by mapper.pl script included in miRDeep2 [19] {http://genomewiki.ucsc.edu/index.php/Hg19_Genome_size_statistics}. miRNA mature and hairpin sequences were obtained from miRBase release 18 {http://www.mirbase.org}. Finally, the resulting fastq files were processed by miRDeep2.pl script. miRNA read counts were extracted from the "read_count" column of the file named"miRNAs_expressed_all_samples_sample_id.csv" file; while sample_id was given automatically by scripts (for sample scripts see Text S1 and for extracted read counts for each miRNA see Table S1). When drawing boxplots, the read count in each sample was normalized such that it had a zero mean and a variance of one. For microarray processing, gProcessedSignal values were extracted from raw data files. gProcessedSignal values were also normalized so that they had a zero mean and a variance of one. Average gProcessedSignal values over probes assigned to common mature miRNA were used to compute the correlation coefficient for NGS and microarray results. The correlation coefficients of logarithmic expression and subtracted expression were computed using only miRNAs with non-negative signals in both NGS and average microarray expression. P-values associated with boxplots were computed using Wilcoxon rank sum test. All bioinformatics computation was performed using functions implemented in R.

To discriminate HCC from non-tumorous tissue when miRNA expression was quantified by NGS, we combined principal components analysis (PCA)-based feature extraction and PCA-based linear discriminant analysis (LDA) [20] [21]. When PCA-based feature extraction was applied, each miRNA was embedded into a two-dimensional space by PCA and M miRNAs located far from the origin (outliers) were selected. Using these selected miRNA, each sample was embedded into a low dimensional space with dimension (M–M'). Samples were then discriminated by LDA using the M' dimensional PC scores. For more details, see Text 2. Novel miRNA candidates were selected from the total set if they satisfied the following criteria: 1) among the novel miRNAs identified by miRDeep2, those with a >80% probability of being a true positive, and 2) the miRNA was reproducibly detected in more than three samples.

Results

Analysis of miRNA sequence reads and reproducibility of NGS analysis

The average number of sequencing reads per sample exceeded 2.2 million, of which approximately 57% mapped to the human reference genome (for more details, see Table S2). A scatter plot of logarithmic miRNA expression measured by NGS and microarray using the first technical replicate of K-177 (K-177_1) is shown in Fig 1.

Table 1. Clinical information of 14 HCC patients analyzed in this study.

code No.	*histological* differentiation	sex	age	HBsAg	anti-HCV	AFP	PIVKA-II	*no tumorous* tissue	NGS analysis	microarray analysis
CU-070	moderately	M	53	(−)	(+)	3510	NI	LC	only HCC	only HCC
CU-083	moderately	M	49	(+)	(−)	143830	0.9	LC	both	only HCC
CU-085	moderately	M	55	(−)	(+)	113	0.06	LC	only HCC	only HCC
CU-087	well	M	62	(−)	(+)	NI	NI	NI	both	only HCC
CU-089	moderately	F	61	(−)	(+)	400	0.06	CH	both	only HCC
CU-091	moderately	M	64	(−)	(+)	5	0.06	CH	only HCC	only HCC
K-023	moderately	M	47	(+)	(−)	3500	2.2	LC	only HCC	only HCC
K-147	poorly	M	65	(−)	(+)	NI	NI	NI	only HCC	neither
K-175	moderately	M	67	(−)	(+)	3.4	32	CH	both	neither
K-177	moderately	M	68	(−)	(+)	13	29	NI	both	only HCC
K-181	well	M	LC	(−)	(−)	5.1	19	NI	both	neither
O-086	moderately	F	64	(−)	(+)	218	32	LC	only HCC	only HCC
O-088	moderately	M	74	(+)	(−)	13.4	7991	LC	only HCC	only HCC
O-089	moderately	M	68	(−)	(+)	8	25	LC	only HCC	only HCC

Abbreviations, moderately; moderately differentiated HCC, well; well differentiated HCC, poorly; poorly differentiated HCC, NI; no information, CH; chronic hepatitis, LC; liver cirrhosis, only HCC; only HCC was analyzed by NGS, both; both tumor and non-tumorous tissue were analyzed by NGS, neither; neither HCC nor non-tumorous tissue was not analyzed.

doi:10.1371/journal.pone.0106314.t001

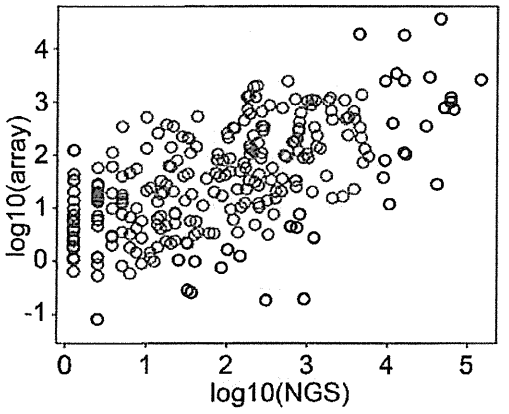

Figure 1. Comparison between logarithmic HCC miRNA expression in NGS (horizontal axis) and microarray (vertical) analysis (K-177_1 means the first technical replicates of code No. K-177). One black circle showed one miRNA. Pearson's correlation coefficient is 0.6059.
doi:10.1371/journal.pone.0106314.g001

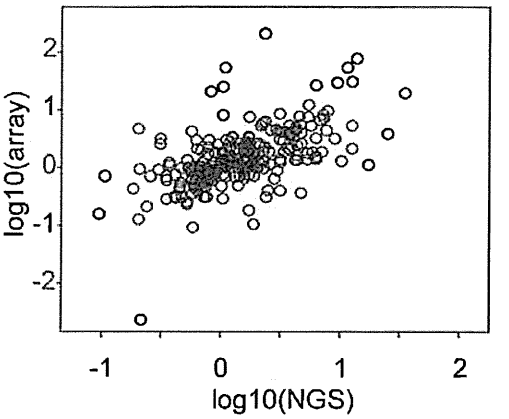

Figure 2. Comparison between differential (K-177 vs. CU-087) logarithmic HCC miRNA expression in NGS (horizontal axis) and microarray (vertical) analysis. Pearson's correlation coefficient is 0.5555.
doi:10.1371/journal.pone.0106314.g002

Although the microarray and NGS expression levels are not perfectly correlated, they are approximately proportional to each other with a positive proportional coefficient. The corresponding scatter plots for the remaining 9 HCC samples are shown in Fig. S1. The similarity in the NGS and microarray miRNA profiling results was relatively independent of the samples considered. The correlation coefficient of logarithmic miRNA expression from 11 HCC miRNA expression profiles as measured by both NGS and microarray was 0.613. This demonstrates that NGS and microarray measurements give similar results.

We next validated the reproducibility of miRNA differential expression across the 11 samples. In general, miRNA expression profiles are not individually evaluated; instead, profiles for distinct samples are analyzed in pairs e.g., compared between tumor and adjacent non-tumorous tissue. Thus, reproducibility between NGS and microarray is more important in differential expression than in any single expression measurement by itself. Fig. 2 shows a scatter plot of differential (K-177 vs. CU-087) logarithmic miRNA expression obtained by NGS and microarray (Fig. S2 shows the full set of scatter plots). Again, we observed that the coincidence between NGS and microarray miRNA profiles was relatively strong irrespective of the sample pair that was considered. The correlation coefficient of differential logarithmic miRNA expression averaged over all pairs of 11 HCC is 0.587. This demonstrates a reasonable level of congruency between miRNA profiling results from NGS and microarray when considering differential logarithmic miRNA expression.

miRNA expression measured by NGS can be applied to diagnosing HCC

In order to discriminate between HCC and non-tumorous tissue, 11 miRNAs quantified by NGS (miR-10a-5p, miR-122-5p, miR-146b-5p, miR-148a-3p, miR-192-5p, miR-22-3p, miR-26a-5p, and miR-27b-3p, miR-10b-5p, miR-143-3p, and miR-21-5p) were chosen by PCA-based feature extraction. The miRNA expression levels in HCC and non-tumorous tissue is shown in Fig 3. The expression level of miR-10a-5p ($p<2.56\times10^{-2}$), miR-122-5p ($p < 1.55\times10^{-3}$), and miR-22-3 ($p<4.64\times10^{-3}$) among the 11 miRNAs differed significantly in the HCC and non-tumorous tissue. miRNA profiling allowed the accurate prediction of HCC with an overall cross-validation accuracy of 90.0% (18/20) by PCA-based feature extraction (Table 2). The p-value and AUC value for diagnostic ability were $<7.22\times10^{-4}$ and 0.92 respectively.

Reproducibility of NGS measurement among technical replicates

We have demonstrated that quantifying miRNA using NGS gives results similar to those obtained by microarray, and that miRNA expression measured by NGS can discriminate HCC from non-tumorous tissue. However, we have found that miRNA profiling using NGS is more accurate in cases where NGS measurement does not vary within multiple technical replicates. For those HCC samples in this study that had more than one technical replicate we validated the reproducibility of NGS miRNA expression between technical replicates. Fig. 4 shows examples of technical replicates (other scatter plots are available in Fig. S3). Among three technical replicates, the correlation coefficients of logarithmic miRNA expression are greater than 0.98. Additionally, the dynamic range is almost 5 digits. This means that technical replicates obtained from NGS measurements are highly reproducible.

Discovery of novel miRNAs in our analysis

NGS detected several miRNA candidates that are not registered in the present miRBase (Rel. 18) (see Materials and Methods for detection criteria, and see Supporting Information for more details about detected miRNAs). We speculate that four precursor miRNAs, hsa-mir-9985, hsa-mir-1843, hsa-mir-548bc, and hsa-mir-9986 and the corresponding four mature miRNAs, hsa-miR-9985, hsa-miR-1843, hsa-miR-548bc, and hsa-miR-9986, were not previously reported because they are not among the miRNAs found at the corresponding genomic coordinates. Fig. 5 shows the sequence of the new miRNA candidates, their alignment with their closest homologous miRNA, and the hairpin structure predicted by RNA-fold with default parameter settings (short reads mapped to these candidate miRNAs are available in Table S3).

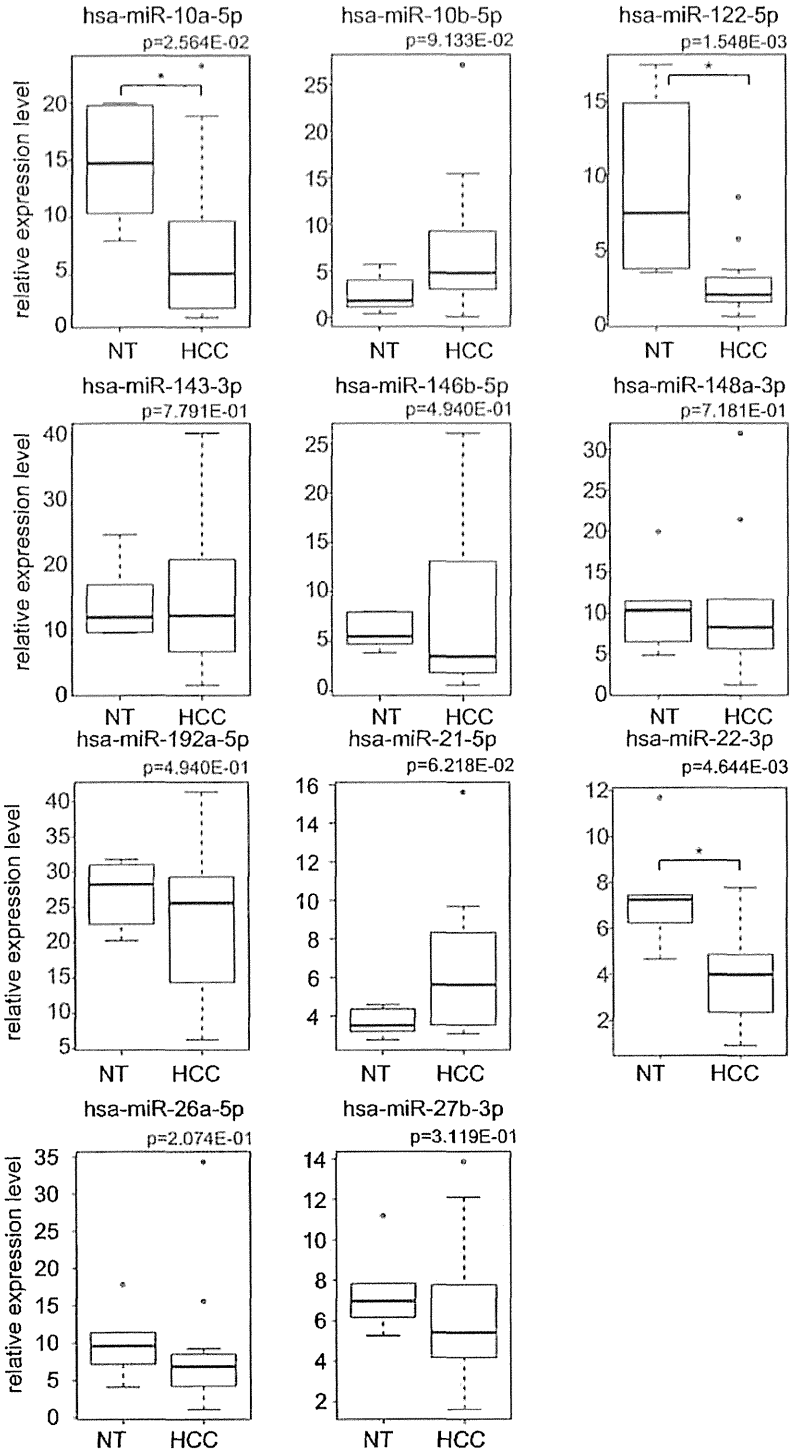

Figure 3. Boxplots of the expression of 11 miRNAs in HCC and non-tumorous tissue obtained by NGS, which were used for the differential analysis. P-values were computed using two-sided Wilcoxon Rank Sum test. Asterisk indicates a significant difference of $p<0.05$ (*).
doi:10.1371/journal.pone.0106314.g003

Table 2. Performance of discrimination between 14 HCC samples and 6 normal tissue samples using miRNA expression obtained by NGS analysis.

		Result	
		Control	**Tumor**
Prediction	Control	12	0
	Tumor	2	6

doi:10.1371/journal.pone.0106314.t002

Discussion

The clinical application of miRNA expression profiling, such as its use as a disease biomarker, has been extensively developed in recent years. This analysis demonstrates that miRNA profiling by NGS has the potential to diagnose HCC with high accuracy. Previous comprehensive analyses of miRNA expression have been performed by microarray; however, the miRBase is currently underdeveloped. An updated miRBase is required to create accurate microarray profiles, and especially because microarray experiments performed using previous version of miRBase are incompatible with microarrays based on the current version. The results from our miRNA expression analysis in HCC suggest that NGS may allow us to overcome this problem. Law et al. has previously reported small RNA transcriptome analysis in HCC by using NGS [18]. However, pre-miRNAs are of a similar length as other more numerous classes of ncRNA, including tRNA and snoRNA, making deep profiling of pre-miRNA sequences difficult [22]. Therefore, this study focused on the analysis on whole miRNA instead of ncRNA.

In order to determine if miRNA expression as measured by NGS technology can discriminate HCC from non-tumorous tissue, we adopted a recently proposed combination of PCA-based feature extraction and PCA-based LDA [20] [21] (for details, see Materials and Methods). Previously, we showed that miRNA expression profiles detected by microarray can accurately discriminate HCC from non-tumorous tissues [7] [23] [24] [25]. Therefore, because NGS produced results similar to those by microarray, and was capable of differentiating HCC from non-tumorous tissues, it is evident that miRNA expression quantified by NGS is as informative as is miRNA expression assessed by microarray. NGS's ability to quantify miRNA expression suggests

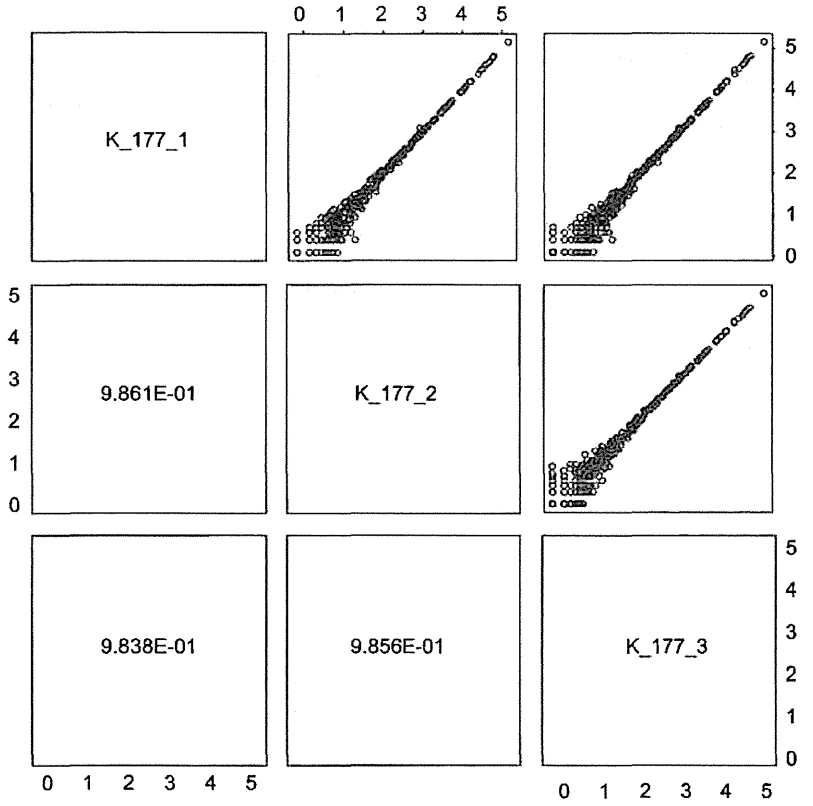

Figure 4. Comparison between logarithmic miRNA expression in HCC and NGS technical replicates (K-177_1 means the first technical replicates of code No. K-177). Pearson's correlation coefficients are greater than 0.9861.
doi:10.1371/journal.pone.0106314.g004